Titre: Title:	Fabrication of polymer microstructured fibers for applications in guiding of optical power, microfluidics and sensing
Auteur: Author:	Ning Guo
Date:	2007
Type:	Mémoire ou thèse / Dissertation or Thesis
Référence: Citation:	Guo, N. (2007). Fabrication of polymer microstructured fibers for applications in guiding of optical power, microfluidics and sensing [Master's thesis, École Polytechnique de Montréal]. PolyPublie. https://publications.polymtl.ca/8437/

UNIVERSITÉ DE MONTRÉAL

FABRICATION OF POLYMER MICROSTRUCTURED FIBERS FOR APPLICATIONS IN GUIDING OF OPTICAL POWER, MICROFLUIDICS AND SENSING

NING GUO
DÉPARTEMENT DE GÉNIE PHYSIQUE
ÉCOLE POLYTECHNIQUE DE MONTRÉAL

MÉMOIRE PRÉSENTÉ EN VUE DE L'OBTENTION
DU DIPLÔME DE MAÎTRISE ÈS SCIENCES APPLIQUÉES
(GÉNIE PHYSIQUE)
AVRIL 2007

Your file Votre référence
ISBN: 978-0-494-53906-4
Our file Notre référence
ISBN: 978-0-494-53906-4

UNIVERSITÉ DE MONTRÉAL

ÉCOLE POLYTECHNIQUE DE MONTRÉAL

Ce mémoire intitulé:

FABRICATION OF POLYMER MICROSTRUCTURED FIBERS FOR APPLICATIONS IN GUIDING OF OPTICAL POWER, MICROFLUIDICS AND SENSING

présenté par: GUO Ning
en vue de l'obtention du diplôme de: Maîtrise ès sciences appliquées
a été dûment accepté par le jury d'examen constitué de:

M. YELON Arthur, Ph.D., président
M. SKOROBOGATIY Maksim, Ph.D., membre et directeur de recherche
M. ANDREWS Mark, Ph.D., membre

Acknowledgements

There are many people that I would like to thank for making this work possible. First of all, I would like to thank my advisor, Professor Maksim Skorobogatiy, for his guide and encouraging me along the way. His personality full of wisdom and forward looking enlightened me to finish my research work. I consider myself very lucky working in Complex Photonic Structures and Processes Group.

I would also like to thank Professor Charles Dubois for offing the opportunity to work in the Chemical Lab and his support. Thanks to Professor Yelon Arthur and Professor Wertheimer Michael for useful discussions and inspirations.

I would like to express my appreciations to Dr.Yan Gao for her advices and intellectual supports. Without her help, this project would not be able to be achieved. Also thanks to Dr.Mahmoud Rajabian, who did lots of work at early stages and made good beginning.

I'm sincerely grateful to Francis Boismenu and Bertrand Gauvreau for their excellent jobs in workshop. Despite their very busy working schedules, they designed and made practical instruments timely, as well as wonderful and valuable routine technical supports. Both of them give me very deep impression. Also thanks Oleg Zabeida for measurement of index and transmission loss of samples. Thank you, Gino Robin, for supports on chemical materials and equipments.

Many thanks to Alireza Hassani, Elio Pone and Alexandre Dupuis for all good times we enjoyed together.

Finally, I credit many accomplishments to my family for their limitless love, understanding and support through the years.

Montreal, Canada

April 1, 2007 Ning Guo

Résumé

Les objectifs de notre étude sont de développer des techniques permettant la fabrication en série de guide d'ondes et fibres microstructures entièrement faits de polymère pour des applications de guidage de lasers haute puissance, la fabrication de capteurs et autres dispositifs microfluidiques.

Au cours de nos activités de recherche, nous avons utilisé différents thermoplastiques pour la fabrication de fibres microstructurées à haut contraste d'indice ainsi que des polymères biodégradables destinés quant à eux à des applications biomdicales. Enfin, l'étirage de préformes multi composantes a été étudié dans le but d'arriver à produire de longues fibres de structure et dimension uniformes.

La première étape du polymère microstructured la fabrication de fibre est fabrication de préforme. Une très large gamme de polymères a été étudiée. Deux différentes combinaisons de polymères ont été choisies pour la fabrication de fibres de Bragg tout polymère: PMMA/PS et PVDF/PC. La cellulose et ses dérivées ont été sélectionnés comme matériaux biodégradables en raison de leur transparence et de leurs propriétés thermiques appropriées. Pour la fabrication des couches alternées des fibres de Bragg de polymère, deux différentes techniques ont été choisies: évaporation de solvant et roulage conjoint de minces films.

La prochaine étape est schéma de fibre. Différents paramètres d'étirage tels ont été étudiés au moyen d'un modèle informatique développé par le groupe de recherche. La section transversale des fibres ont été examinées à un microscope optique. En plus du procédé d'étirage unique, un procédé d'étirage en deux étapes a été exploré dans le but d'affiner les structures obtenues et ainsi permettre l'emploi de ces fibres dans le visible et le proche infrarouge.

Les techniques élaborées pour la fabrication de MOF de polymère ont été démontrées efficaces et non onéreuses.

Abstract

The goals of my study are to develop series techniques to fabricate all-polymer waveguide and microstructured fiber for applications in high power laser guiding, microfluidics and sensing.

In my research I investigated on various thermoplastics to create high indexcontrast polymer microstructured optical fiber. I also investigated the use of biofunctional thermoplastics, such as biodegradable polymers, for applications in medical field. Finally, the drawing of multicomponent material preforms has be studied on the aim of producing long fibers of stable diameter and microstructure.

The first step of polymer microstructured fiber manufacture is preform fabrication. A very wide range of polymer materials was studied from conventional optical polymers. Two pairs of polymer are chosen for all-polymer Bragg fiber: PMMA/PS and PVDF/PC. Cellulose and its derivatives are selected as biodegradable material because of their optical transparency and good thermal properties. Two methods are chosen to make polymer Bragg fiber preform: solution evaporation and co-rolling method.

The next step is fiber drawing. The drawing parameters were tested to obtain good quality fiber. The cross-section of fibers were examined by an optical microscope. The images show that the fibers successfully maintained the hollow and layer structure. Besides one-step drawing, a two-step drawing technique was carried out to make thinner individual layer thicknesses for working in infrared or visible wavelength.

The techniques we developed in mPOF fabrication are proved effective and low cost. They provide the basic platform to manufacture complex polymer microstructured optical fibers.

Condensé en Français

Les fibres optiques microstructurées (MOF) représentent un champ de recherche très dynamique et promettent une variété d'amé liorations importantes en télécommunications, procédés industriels ainsi que dans le domaine biomédical. Comme matériaux de fabrication de telles fibres, les polymères constituent une bonne option car ils permettent la fabrication de structures difficilement ralisables en verre de silice, par exemple. Les polymères offrent également un vaste éventail de possibilités technologiques, notamment par la grande variété de dopants disponibles.

Les objectifs de notre étude sont de développer des techniques permettant la fabrication en série de guide d'ondes et fibres microstructures entièrement faits de polymère pour des applications de guidage de lasers haute puissance, la fabrication de capteurs et autres dispositifs microfluidiques. Au cours de nos activités de recherche, nous avons utilisé différents thermoplastiques pour la fabrication de fibres microstructurées à haut contraste d'indice ainsi que des polymères biodégradables destinés quant à eux à des applications biomdicales. Enfin, l'étirage de préformes multi composantes a été étudié dans le but d'arriver à produire de longues fibres de structure et dimension uniformes, Cette étude porte à la fois sur la fabrication de la préforme, une réplique de grande taille de la fibre désirée, ainsi que sur son étirage en une fibre de diamètre 10 à 1000 fois inférieur.

Avant la fabrication de préformes, une attention particulière a dû être porte sur le choix des matériaux, la comparaison de leurs propriétés ainsi que leur mise à l'essai. Une très large gamme de polymères a été étudiée, des produits conventionnels jusqu'à ceux qui n'ont fait leur apparition que tout récemment. Certains polymères rarement utilisés pour la fabrication de composants optiques tels que le polyvinylididene fluoride(PVDF) ont aussi été considér és en raison de leurs propriétés particulières. Des matériaux biocompatibles ont aussi été intégrés dans la fabrication de fibres optiques pour d'éventuelles applications de guidage et détection dans le domaine médical.

Deux différentes combinaisons de polymères ont été choisies pour la fabrication de fibres de Bragg tout-polymre. La première est de bonne compatibilité et performance optique et est constituée de polymethylmetacrylate (PMMA) et de polystyrene (PS). La seconde, faite de PVDF et de polycarbonate (PC), résiste à de plus hautes températures et possèdes des propriétés intéressantes pour le guidage d'ondes THz. La cellulose et ses dérivées, acide polylactique (PLA) et polycaprolactone (PCL), ont été sélectionnés comme matériaux biodégradables en raison de leur transparence et de leurs propriétés thermiques appropriées.

Puisque les fibres microstructurées sont de construction significativement différente de celle des fibres conventionnelles, de nouvelles techniques ont dû tre développées pour la préparation des préformes. Pour la fabrication des couches alternées des fibres de Bragg de polymère, deux différentes techniques ont été choisies. L'une par évaporation de solvant et l'autre, par roulage conjoint de minces films. La première méthode consiste à déposer un polymère dissout dans un solvant sur la face intérieure d'un tube creux et de répéter l'opération en alternant les polymères déposés. Le défi est de trouver la bonne paire de solvants permettant de ne pas altérer les couches précédemment déposées lors de l'application d'une nouvelle couche. Les paramètres d'évaporation tels que la température du tube, la concentration en polymère des solutions et le débit de gaz de séchage ont été optimisés pour permettre l'obtention de couches uniformes et de bonne qualité.

L'autre méthode, le roulage conjoint, consiste à rouler conjointement de minces films commerciaux ou fabriqués sur place autour d'un axe et de solidifier thermiquement le rouleau obtenu. Nos travaux on insisté sur le procédé de roulage ainsi que sur la fabrication de films sur mesure, dans nos installations. Nous avons con¸cu et fabriqu é les équipements nécessaires à la production de tels films ainsi qu'à leur roulage conjoint.

Des préformes à deux coeurs ont été fabriquées au moyen d'un empilement de tubes thermoplastiques biodégradables. La fibre obtenue de cette préforme intègre les

fonctions de guidage et détection de lumière, et, potentiellement, d'apport et dosage de médication. Différentes préformes de ce type ont été investiguées, soit à structure poreuse et à gaines optique double.

Les différentes préformes ci-haut mentionnées ont toutes été étirées en de fines fibres au moyen de notre tour d'étirage. L'emploi combiné de plusieurs polymères pour la fabrication de fibres creuses rend le procédé d'étirage complexe. Différents paramètres d'étirage tels que la température du four, la vitesse d'étirage et la vitesse d'apport ont été étudiés au moyen d'un modèle informatique développé par le groupe de recherche. Une fois la fibre obtenue, la section droite de celle-ci a été caractérisée au moyen d'un microscope optique. En plus du procédé d'étirage unique, un procédé d'étirage en deux étapes a été exploré dans le but d'affiner les structures obtenues et ainsi permettre l'emploi de ces fibres dans le visible et le proche infrarouge. Afin d'obtenir des images de section droite de bonne qualité, une cliveuse à fibre a été développée et fabriquée. Celle-ci tranche la fibre au moyen d'une lame chauffante. La température de la fibre et celle de la lame peuvent être contrôlées indépendamment, de plus que la tension appliquée sur la fibre, la vitesse et l'angle de coupe. La préservation de la structure de la préforme a pu être démontrée par ces inspections.

Bien que les pertes en transmission des fibres microstructurées tout-polymère développées ne soient pas compétitives face à celles de fibres conventionnelles, cellesci offrent malgré tout des propriétés de guidage intéressantes pour des applications spécifiques. Les techniques élaborées pour la fabrication de MOF de polymère ont été démontrées efficaces et non onéreuses. Elles constituent le point de départ vers la fabrication de structures plus complexes pour des domaines d'applications variés tels que les télécommunications, les procédés industriels ainsi que le secteur biomédical.

Table of Contents

Acknowledgements IV

Résumé V

Abstract VI

Condensé VII

Table of Contents X

List of Tables XII

List of Figures XIII

List of Appendices XVI

List of Abbreviations XVII

Introduction **1**

Chapter 1 Material Selection **16**

1.1 Polymers for photonic crystal Bragg optical fibers 16

1.2 Polymers for biocompatible/biodegradable optical fibers 19

Chapter 2 Preform Fabrication Methodology **21**

2.1 Consecutive solvent evaporation method 21

2.1.1 Deposition setup 21

2.1.2 Choice of substrate 23

2.1.3 Deposition process 26

2.2 Co-rolling method 27

2.3 Powder packing and solution casting methods 27

Chapter 3 Fiber Drawing **29**

3.1 Introduction 29

3.2 Draw process and draw tower 29

3.2.1 Drawing procedure and parameters 31

3.3 Microstructured preform drawing 33

3.3.1 Drawing of capillaries from a pure PMMA tube 33

3.3.2 Drawing of Bragg fibers from the preform made by solvent evaporation coating method 37

3.3.3 Drawing of Bragg fibers from the preform made by co-rolling method 40

Chapter 4 Biodegradable Microstructured Fibers Drawing and Characterization **43**

4.1 Polymer fiber made with PLA/CA material combination 43

4.2 Biodegradable cellulose-based microstructured fiber 44

4.3 Biodegradable microstructured optical fiber drawing 48

Chapter 5 Conclusions and Discussions **49**

5.1 Summary of accomplishments 49

5.2 Future directions 50

REFERENCES 51

APPENDICES 54

List of Tables

Table. 1	Polymer materials studied in the project	10
Table. 1.1	Polymer material pairs for Bragg optical fiber fabriaction	17
Table. 1.2	Orthogonal solvents for the two pairs of polymer	18
Table. 1.3	Table of biocompatible/biodegradable polymer studied in the project	20
Table. 2.1	Comparison of thermal expansion coefficient for different cladding mterials	24
Table. 3.1	Typical drawing parameters for PMMA tube	35
Table. 3.2	Summary of draw ratio and collapse ratio for selected fiber samples	38
Table. 3.3	Fiber drawing temperatures for preforms with different ratios of PMMA and PS polymer	41
Table. 4.1	Drawing parameters for pure cellulose butyrate (CB) tube	45

List of Figures

Figure. 1 Cross-section and index profile of the step and graded index POFs 2

Figure. 2 The dimension of POF in comparison with GOF 3

Figure. 3 Historical outline of different photonic crystal fibers, (a)airsilica MOF (Kaiser etal,1974); (b)photonic crystal MOF (Russell et al,1996); (c)photonic bandgap MOF (Cregan et al,1999) 4

Figure. 4 Cross-section of two typical microstructured fiber types: (a)indexguiding fiber; (b)air-guiding fiber 5

Figure. 5 Two types of hollow photonic crystal fiber. (A)microstructured hollow fiber; (B)hollow Bragg fiber 6

Figure. 6 Cross-section of a hollow core Bragg fiber 6

Figure. 7 First polymer microstructured optical fiber 8

Figure. 8 Capillary stacking technology for preform fabrication 11

Figure. 9 Preform fabrication methods: (a) CO_2 laser drilling; (b) stacking disks; (c) extrusion. 11

Figure. 10 Schematic of the layer-by-layer deposition process. (a)Preheat the cladding tube; (b)Inject one polymer solution; (c)Rotate the cladding to form an individual layer of a uniform thickness; (d)Continue with deposition of the next layer. 12

Figure. 11 Schematic of co-rolling process. (a)two polymer films and a mandrel core; (b)co-rolling the films on the outside core; (c)the resultant preform . . 13

Figure. 12 Schematic of a stacking process. 13

Figure. 13 Schematic of a porous preform 14

Figure. 14 Schematic of a optical fiber draw tower 14

Figure. 1.1 Schematic of the Doctor Blade technique 17

Figure. 1.2 Interface of a 3 layers polymer multilayer film fabricated with Doctor Blade technique(PS/PMMA/PS) 17

Figure. 1.3 Micrograph of 3-layer polymer film (PS/PMMA/PS). Various imperfections on a surface are clearly visible 18

Figure. 2.1 Schematic of a layer-by-layer deposition system. It consists of a rotation coater and delivery sub-systems 22

Figure. 2.2 Image of a rotation coater sub-system 22

Figure. 2.3 Image of Delivery System 23

Figure. 2.4 Polymer film peeled off from the glass tube. Choice of a cladding tubes is very important 24

Figure. 2.5 Polymer cladding tube. Structure of the interface between cladding tube and polymer multilayer 25

Figure. 2.6 Pretreatment of polymer cladding tube is critical for the quality o f resulting preform. Cracks in the non-treatment tubes. (A)PC tube; (B)PMMA tube 26

Figure. 2.7 Images of biodegradable fiber preform. (A)cross-section of allcellulose preform fabricated by powder packing; (B)all-cellulose preform by solution casting 28

Figure. 3.1 Image of polymer optical fiber draw tower in our laboratory 30

Figure. 3.2 Components of a draw tower. (a)2 zone oven; (b)tractor; (c)laser micrometer 31

Figure. 3.3 (A)C_r as a functional of draw ratio D_r, solid line correspond to multilayer preform, dotted lines correspond to a simple tube with the same thickness as multilayer preform, dashed lines represent the curves of a constant outer diameter. (B)schematic shapes of hole collapse while C_r=1,0.6,0 33

Figure. 3.4 Image of a PMMA tube. The OD is 31.75mm, the wall thickness is 6.35mm and the length is 450mm 34

Figure. 3.5 Images of a neck-down zone of a PMMA tube. (a)when drawing without degassing, many bubbles were in the tapered region. (b)when degassed, there were no bubbles 35

Figure. 3.6 Fiber diameter fluctuation during drawing process 36

Figure. 3.7 The cross-sections and fitted images of fibers drawn at draw different speeds (Vd). (A)2100 – 2300(mm/min); (B)3200 – 3400(mm/min); (C)4000 – 4300(mm/min) 37

Figure. 3.8 Schematic and cross-section images of a Bragg fiber fabricated by solvent evaporation method. The number of multilayer is 10 38

Figure. 3.9 Due to imperfect solvent trapped in preform, bubbles appeared during drawing 39

Figure. 3.10 Preform weight Loss in solvent extraction experiment 39

Figure. 3.11 Drawing Bragg fiber preform fabrication by solvent evaporation 40

Figure. 3.12 The cross-section of PMMA/PS Bragg. The fiber diameter is 250um 40

Figure. 3.13 The cross-section of a Bragg fiber drawn by two-step technique 42

Figure. 3.14 Cross-section of PVDF/PC Bragg fiber 42

Figure. 4.1 Biodegradable PLA/CA preform and cross-section of fiber 44

Figure. 4.2 Double-core fiber packed with high molecular weight(M_w _ 370, 000) HPC powder. (A)Tapered preform; (B) The Cross-section of fiber 46

Figure. 4.3 Images of fiber fabricated by powder packed with lower molecular weight HPC powder M_w _ 80, 000. (A)Cross-section of porous double-core preform; (B) and (C)fiber cross-section 46

Figure. 4.4 Biodegradable polymer fiber from a PCL/CB combination. (A)Drawn polymer fiber; (B)The cross-section of a fiber 47

List of Appendices

Appendix A

Consecutive Solvent Evaporation and Co-Rolling Techniques for Polymer Multilayer Hollow Fiber Preform Fabrication. 54

Appendix B

The prospective for the biodegradable microstructured optical fibers . . . 64

List of Abbreviations

2D	Two-dimension
CA	Cellulose Acetate
CB	Cellulose Butyrate
COC	Cyclic Olefin Copolymer
GI	Graded-index
GOF	Glass optical fiber
HF	Holey fiber
HF	Hydrofluoric acid
HPC	Hydroxypropyl cellulose
IR	Infrared
ID	Inside diameter
MCVD	Modified chemical vapor deposition
MOF	Microstructured optical fiber
mPOF	Microstructured polymer optical fiber
OD	Outside diameter
PCF	Photonic crystal fiber
PC	Polycarbonate
POF	Polymer optical fiber
PCL	Polycaprolactone
PF	Perfluorinated
PLA	Polylactic acid
PMMA	Polymethylmet acrylate
PS	Polystyrene
PVDF	Polyvinylididene Fluoride
RI	Refractive index
SI	Step-index
T_g	Glass transition temperature

Introduction

This chapter provides an introduction to optical fiber and microstructured optical fibers. The brief history and basic characteristics of conventional and microstructured optical fiber are reviewed in sections 1.1, 1.2, and 1.3. In section 1.4, the outline of topics of the master project are presented including material selection, preform fabrication and fiber drawing techniques.

0.1 Optical fiber and polymer optical fiber

Polymer optical fiber (POF) was introduced by DuPont in the 1960s at approximately the same time that glass optical fiber (GOF) was suggested as transmission medium for optical communications (Nalwa, 2004). The first product was a step-index fiber with a polymethylmethacrylate (PMMA) core and a fluoropolymer cladding. Mitsubishi Rayon in Japan developed Dupont's extrusion technology for POF, and led to the introduction of Eska^{TM} (Co., 1974), which had a PMMA core and poly(fluoroalkyl methacrylate) cladding as well. The attenuation was 300dB/km and applicability was limited to low end uses like illumination.

In 1970, glass fiber loss was demonstrated below 20dB/km in the wavelength region near 1μm (Kapron et al., 1970). At the end of 1970s, fiber attenuation was reduced to 1dB/km at wavelength 1.3μm and the era of fiber-optic communications commenced. In the meantime, the loss of PMMA-based POF also had been reduced to about 160dB/km at a wavelength of 650nm by process improvement. In the middle of the 1980s, it was further reduced to about 20dB/km at 680nm by using deuterated

PMMA(PMMA-d8) (Kaino et al., 1983).

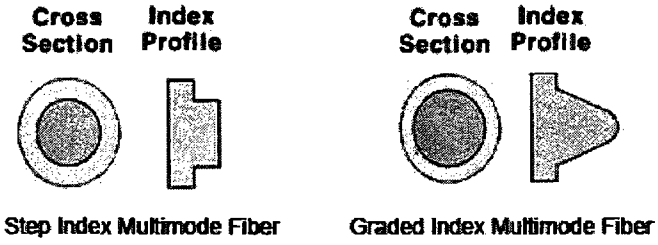

Figure 1: Cross-section and index profile of the step and graded index POFs

All the above-mentioned POFs were step-index (SI) POFs. The first graded-index (GI) POF was manufactured by Ohtsuka and Hatanaka in 1976 by heat-drawing a graded-index polymer rod (Ohtsuka and Hatanaka, 1976). Until early 1980s, graded-index polymer rods, which have different cross-section and index profile from conventional optical fibers as shown in Figure1, were fabricated by two methods: two-step copolymerization (Co., 1976) and photo-copolymerization (Ohtsuka and Nakamoto, 1976). Later, in 1988, when the interfacial-gel polymerization methods was invented, GI-POFs could be made with much smaller attenuation (Koike et al., 1989). The theoretical attenuation limit of perfluorinated (PF) GI-POFs was estimated to be as low as 0.3dB/km (Nalwa, 2004), which is comparable to that of silica fiber in the near infrared wavelength. Transmission speeds greater than 10Gbit/s at the near infrared region have been reported (Chen et al., 2000).

During the past two decades, the rapid advancement of optical fiber communication led POFs to many applications in high-bandwidth data transmission for local area networks or home networks despite its relatively high optical loss compared to glass fiber (Ishigure et al., 1996). Due to the much larger core diameter, on the order of 1mm compared to about 5-10μm for single-mode GOFs, using POFs make splicing and coupling much easier, thus offering a significant economic advantage. Figure 2 shows the dimension of polymer optical fiber in comparison with glass optical fiber.

Recently, with the extensive research on both material and fabrication technology,

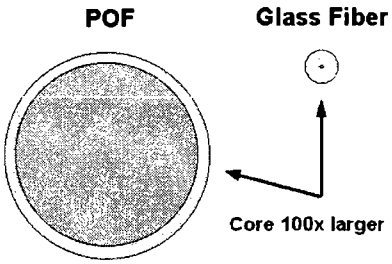

Figure 2: The dimension of POF in comparison with GOF

SI and GI-POFs spun many emerging areas of application. For example, Tayag reported GI-POFs used as an optical fiber amplifier by doping its core with organic dyes (Tayage et al., 1997). Plastic fibers could be also made as essential components of a selfoc lens array in fax machines and scanners (Toyoda et al., 1995). In addition, because of polymer's biocompatible property, POFs offer a wide range of potential applications in a biomedical field.

0.2 Photonic crystal and microstructured optical fiber

Microstructured optical fibers (MOF), holey fibers (HF), and photonic crystal fiber (PCF) come in a variety of different shapes, sizes, and distributions of air-holes. The earliest work reported by Kaiser, as shown in Figure3(a), demonstrated that the microstructured optical fiber made from silica can be low loss (Kaiser and Astle, 1974). At the end of the 1980s, the development of photonic crystals offered a powerful means of modifying transmission characteristics of light (Yablonovitch, 1987). In the 1990s, a number of research groups worked to extend the working wavelength to the infrared (IR) and visible wavelengths by scaling down the feature sizes to the micron scale. Several years later, Russell and his team demonstrated a so-called photonic crystal fiber as shown in Figure 3(b) (Knight et al., 1996). For the first time, optical guidance within a silica fiber with a complex holey cladding structure was demonstrated. In 1997, a true photonic bandgap optical fiber, which was able to

guide light in a central air-core region surrounded with a periodic array of air-holes (Figure 3(c)), was demonstrated by Cregan et al (Cregan et al., 1999).

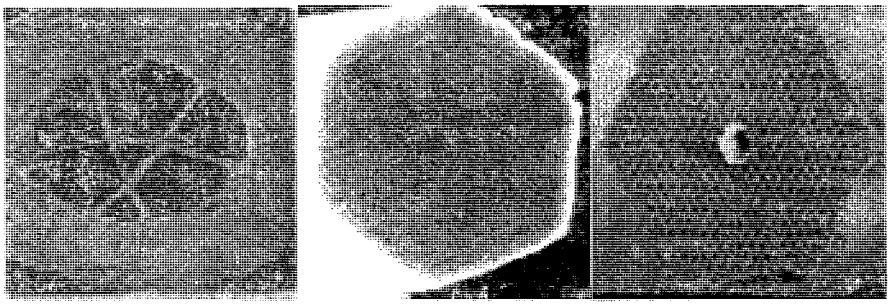

(a) (b) (c)

Figure 3: Historical outline of different photonic crystal fibers, (a)air-silica MOF (Kaiser etal,1974); (b)photonic crystal MOF (Russell et al,1996); (c)photonic bandgap MOF (Cregan et al,1999)

Generally, one distinguishes two guiding mechanisms in microstructured optical fiber - index-guiding and bandgap-guiding. The first one is a modified form of total internal reflection guiding, as the effective refractive index in the solid core region of a fiber is greater than that of surrounding air-filled region (Tanya and Ebendorff-Heidepriem, 2006). A typical index-guiding MOF is shown in Figure 4(a) (Richardson et al., 2005). The hole diameter (d) and hole-to-hole spacing (Λ), which are critical parameters when a hexagonal lattice of air holes is used, are typically on the scale of the wavelength (λ) of light. The large index contrast between core glass and cladding air holes makes the effective cladding index strongly wavelength dependent. This is fundamentally different compared to a conventional SI or GI optical fiber, and, this leads to the fiber highly unusual optical properties.

A typical fiber is shown in Figure4(b) (Richardson et al., 2005), where light is localized by the bandgap of a periodic cladding. Such a fiber is able to guide the light within an air core which cannot be achieved with a conventional optical fiber cladding (Tanya and Ebendorff-Heidepriem, 2006).

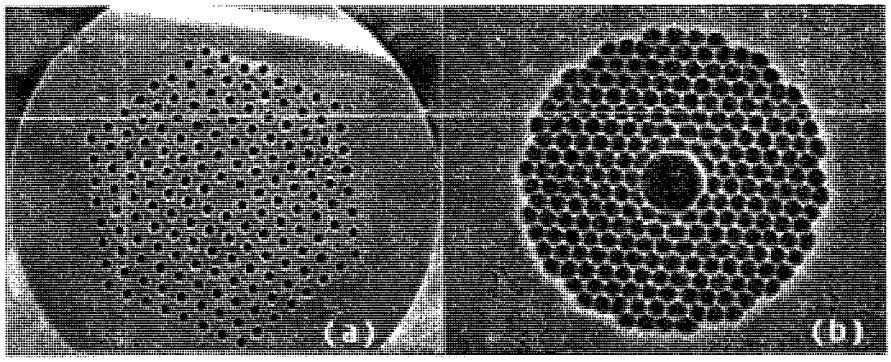

Figure 4: Cross-section of two typical microstructured fiber types: (a)index-guiding fiber; (b)air-guiding fiber

In recent years, the research in the field of photonic bandgap fiber have progressed rapidly. These optical fibers offer many novel optical properties that cannot be provided by conventional optical fibers, such as, unique dispersion characteristics (Ranka et al., 2000), nonlinearity (Knight et al., 1998), and infinitely single mode region (Birks et al., 1997) as well as the integration of microfluidics directly into the fiber structure which is of importance to sensoring application (Dupuis et al., 2007). The main disadvantage of air-guided and index-guided PCFs is higher loss compared with the conventional single-mode optical fibers as well as highly complicated fabrication process.

0.3 Hollow photonic crystal Bragg fiber

One significant advantage of PCFs is their abilities to guide light in the air or other low refractive index core through the photonic bandgap effect. Photonic bandgap guidance requires a periodic structure within the cladding, such as a periodic arrangement of holes which can be described as a two-dimensional (2D) photonic crystal (Figure 6(a)) or a one-dimensional (1D) microstructured cladding (Figure 6(b)) (Temelkuran et al., 2002). Experimental realization of a 1D photonic crystal cladding is shown in Figure 6 (Richardson et al., 2005).

Bragg fiber cladding consists of alternating layers of high and low reflective index

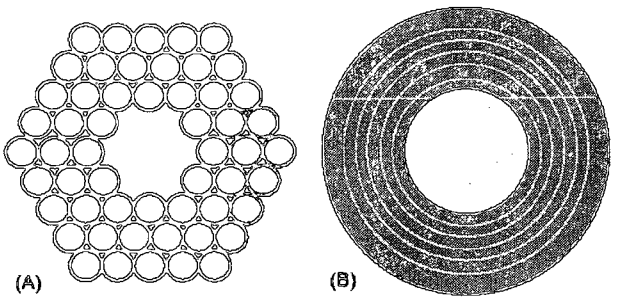

Figure 5: Two types of hollow photonic crystal fiber. (A)microstructured hollow fiber; (B)hollow Bragg fiber

materials. The geometry of periodic reflective index enable a guidance of any desirable wavelength from the visible to THz. Practical application of hollow core Bragg fiber is CO_2 laser power delivery at mid-IR wavelength (Temelkuran et al., 2002).

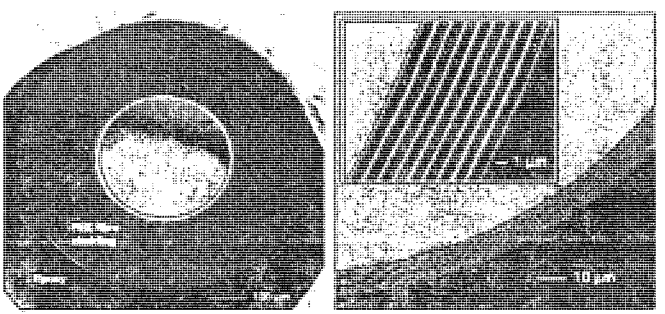

Figure 6: Cross-section of a hollow core Bragg fiber

0.4 The objective and challenges of the project

Study of microstructured optical fibers (MOF) is a very active field of current research. Novel structures are constructed to enable various applications. However, there are a number of technological challenges for MOF fabrication from preform manufacture to fiber drawing impeding their commercialization. The main goal of my study is to develop novel techniques based on the preform drawing methodology for the fabrication of polymer microstructured optical fiber. With these techniques, single or multi-polymer material combination could be used to form more complex

fiber geometries. The following are the main challenges in my work.

0.4.1 Material selection

Both index-guiding and air-guiding MOFs can be made from single material or from combination of several materials. Silica glass, soft glass, and polymers are possible materials for microstructured optical fiber. Germanium-doped silica and pure undoped silica are the materials used for core and cladding of conventional solid optical fibers with losses of order 0.2dB/km (Wang et al., 2006). Up till now, the vast majority of microstructured optical fibers have been manufactured from undoped silica glass. Main disadvantages of silica material include absorbtion about $2\mu m$; low intrinsic nonlinearity which is not suitable for active device application (Tanya and Ebendorff-Heidepriem, 2006); and mechanical brittleness.

Soft glasses have significantly lower melting temperature than silica glasses. A number of soft glasses transmit at wavelengths extending beyond that of silica into the mid-infrared (mid-IR). Microstructured fibers made from such materials offer a new means of delivering light at mid-IR wavelengths (Tanya and Ebendorff-Heidepriem, 2006). Moreover, such glasses are typically highly nonlinear making them good candidate for active applications.

In our group we use polymers as materials of MOF. A polymer is a chemical compound with high molecular weight consisting of a number of structural units linked together by covalent bonds. There are two basic materials types: thermopolymer, which cannot be resoftened or reshaped after being subjected to heat and pressure; and thermoplastic polymers, which can be repeatedly softened and remolded by heat and pressure. Polymers that contain a single repeating unit are called homopolymers. Those contain more different more units are called copolymers.

In 2001, first polymer microstructured optical fiber (mPOF) was developed as shown Figure 7 (Eijkelenborg et al., 2001). mPOF offers many advantages over their glass competitors as the fabrication is easier and more economical on both preform

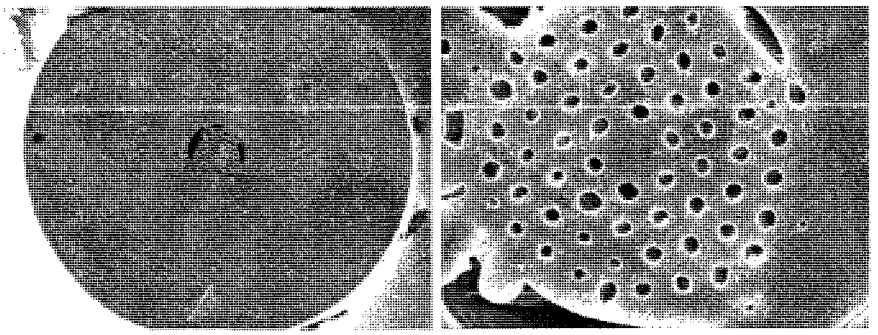

Figure 7: First polymer microstructured optical fiber

and drawing stages. In addition the capillary stacking methods used in glass POF, many traditional polymer process technologies, such as extrusion, drilling, injection moulding, or polymerization in a mould, can be applied. That means nearly limitless possibilities of hole shapes and sizes in any desired arrangement. So far, a much wider variety of mPOFs compared to glass POFs has been demonstrated, including single-mode, highly-birefringent, twin-core, graded-index, and hollow-core mPOFs.

The drawing procedure of mPOFs is easier compared to silica glass optical fibers due to lower drawing temperature and typically smaller polymer surface tension. The viscosity of PMMA and silica are of similar magnitudes at their respective draw temperatures. The surface tension of PMMA is about $0.032N/m$ and a typical viscosity is about $5 \times 10^6 Pas$ (Barton et al., 2004) during drawing. In comparison, silica glass has a surface tension of about $0.30N/m$ and a typical viscosity of $3.6 \times 10^6 Pas$ at the draw temperature (Fitt et al., 2001). Thus PMMA's surface tension is an order of magnitude lower than that of silica (Wu, 1970). Thus the distortion and collapse due to surface tension effects are easier to be minimized to allow fabrication of the fine-scale mPOFs.

Additionally, a solution doping allows dopants to be introduced into the polymer matrix. The ability to dope polymers with dyes of rare-earth ions provides possibility of fabrication optical fiber for fiber lasers and fiber gratings (Webb et al., 2005). Finally, polymers offer outstanding mechanical properties and are generally more biofriendly than glasses.

As a homopolymer, PMMA has a refractive index of $n_D = 1.492$ which can be turned by adding low molecular weight dopants. This polymer works stably up to 85°C in dry air. Higher temperatures, especially in humid conditions, cause rapid degradation of the polymer and reduce the service life to a few months. The transmission window at wavelength of 550-650nm is suitable for data communications. Conventional polymer optical fiber that use PMMA as a core material has theoretical attenuation of 55dB/km (570 nm), and typical measured attenuation of 100-500 dB/km. The glass transition temperature (Tg) for PMMA homopolymer is 105°C, which is dependent slightly on the structure and molecular weight (Pratt, 2005).

There are many choices of polymers for mPOF fabrication besides PMMA. Very attractive properties like higher working temperature, better transparency, wider transmission wavelength ranges, higher stability etc, are enabled by various polymer materials. For example, polyvinylidence fluoride (PVDF) proves to be a better material for terahertz waveguides (Hidaka et al., 2005). Biodegradable polymer can be completely converted to biologic products (biogas, humic matter, biomass) in biologically active environment within a suitable period of time. Microstructured optical devices made from biodegradable polymers offer a possibility of novel in vivo application.

Finally, for the fabrication of Bragg fibers, for which refractive index-contrast is important, several different polymers combinations can ge easily identified. In Table table0.4.1 (Aldrich, 2006b), we summaries all the polymers used in this works.

0.4.2 Fabrication technology

In practice, the traditional preform-drawing technique has the advantages of simplicity and versatility. Because thermal exposure during the heat-drawing process is limited, the degradation of polymer is less compared to the continuous extrusion method. In addition, the preform drawing process is easy to modify and the materials can be combined with other organic or none-organic materials.

Table 1: Polymer materials studied in the project

Material	T_g(°C)	Density(g/ml)	Refractive index
PMMA	105	1.19	1.49
PS	100	1.05	1.59
PC	149	1.20	1.58
PVDF	-38	1.76	1.42
CA	100	1.30	1.48
CB	100	1.25	1.48
PCL	-60	1.15	1.52
PLA	49	1.18	1.45

Generally, the fabrication process of a mPOF can be divided into two stages: preform manufacture and fiber drawing. The first stage is the production of a preform, which is in principle a large scale version of required fiber structure. In the second stage, the preform is drawn into a fiber by the heat-drawing process. The preform step is often the most challenging fabrication step of the whole fabrication process.

0.4.3 Preform fabrication

Microstructured optical fiber has complicated structure in its cross-section, as a result, it requires a complex fabrication process. Standard method is a capillary stacking technique as shown in Figure 8. In detail, high optical quality, uniform silica capillary are stacked layer by layer around a glass rod in a hexagonal configuration. When index-guiding MOF preform is made, the central glass rod is of higher refractive index forming a waveguide core. The stacking procedure is very flexible and allows, for example, the fabrication of active fibers by using doped core rods. One of the disadvantages of this technique is contamination of the glass rods during stacking, as even small amount of dust on the glass surface can result in significant attenuation increase as well as breakage during fabrication.

Another technology for perform structuring is direct longitudinal drilling of cavities in bulk materials using laser or mechanical devices. The process can be applied

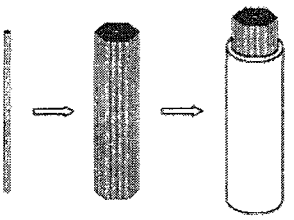

Figure 8: Capillary stacking technology for preform fabrication

to many diverse optical materials, including polymers, soft glasses or silica glasses, and it permits a wide range of geometries. This technology may also be used as an intermediate step for the production of individually machined disks that can be stacked to form the final cylindrical shape preform or for the technique of co-axially combining machined rods and tubes with longitudinal grooves that line up to form the lattice (Wang, 2003) (Hasegawa, 2004), as shown in Figure 9(B). The disadvantages of drilling include the introduction of surface roughness and limitation of a maximum preform length.

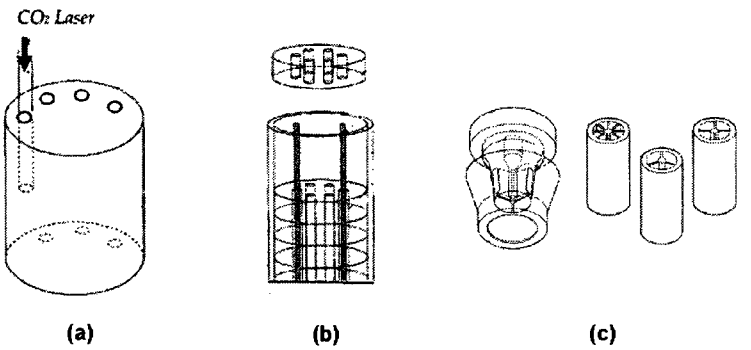

Figure 9: Preform fabrication methods: (a) CO_2 laser drilling; (b) stacking disks; (c) extrusion

Extrusion methods of MOF manufacture have been applied to soft-glasses and polymers with low softening points (Ebendorff et al., 2006). This technology allows fabrication of a structured fiber preform with millimetre-scale features directly from bulk glass or polymer billets by using the die that defines the preform geometry during fabrication. From Figure 9(C), nearly any structure is possible because there are no

restrictions on hole and circular shape. The problems is that that extrusion procedure is an additional thermal process, which may lead to the deformation of the preform and final fiber. Also the design of degas for complex fiber is challenge.

In our project, three fabrication methods of polymer preform are investigated. The first one uses layer by layer polymer deposition by solvent evaporation on the inside of a cladding tube. The second one uses co-rolling of polymer films around a core mandrel. Finally, the third one is a polymer capillary stacking technique.

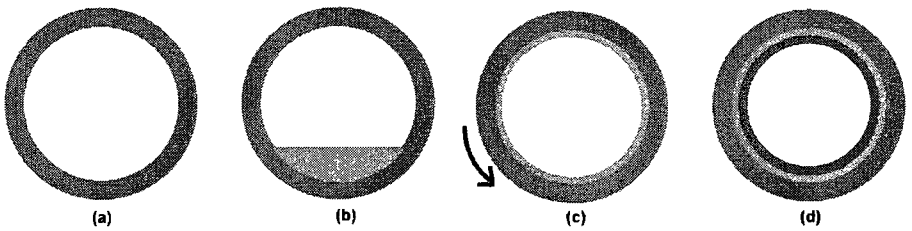

Figure 10: Schematic of the layer-by-layer deposition process. (a)Preheat the cladding tube; (b)Inject one polymer solution; (c)Rotate the cladding to form an individual layer of a uniform thickness; (d)Continue with deposition of the next layer

The first method is a novel technology to enable two polymers material combinations by consecutive evaporation of polymer solutions on the inside of a rotating cladding tube to create a high index-contrast multilayer inside of a fiber. Fiber material designs require a pair of polymers which are not only thermally and chemically compatible but that also have appropriate optical characteristics for guidance. Evaporation parameters such as cladding tube temperature, polymer concentration, purging gas flow rate has to be optimized to deposit a large number of smooth polymer films.

The second method to make multilayer preform uses a co-rolling technique that rolls polymer films around a mandrel and then solidify in the oven at the temperature higher than material's glass transition temperature. The prerequisite for this technique is the availability of high quality polymer films. Commercial PMMA, PS, PVDF, PC, Cellulose film and home-made PLA films were used to make preforms.

The third method is a capillary stacking method. Commonly, a preform stack is assembled using stacking of individual capillary tubes in the form of the desired PCF.

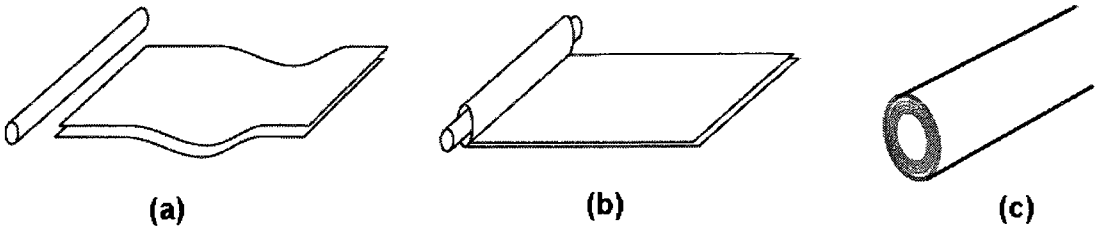

Figure 11: Schematic of co-rolling process. (a)two polymer films and a mandrel core; (b)co-rolling the films on the outside core; (c)the resultant preform

The stack is then over-clad by using a large diameter tube or capillary, which keeps the individual elements in their relative positions in the stack.

To reduce final fiber dimensions, we have also applied stacking method of the two-step fiber drawing. After the first drawing, the fiber is re-stacked with other PMMA capillaries into a larger size polymer tube as shown in Figure 12. Thus, the total drawdown ratio of a two-step process can be much larger than only one-step drawing resulting in much smaller fibers.

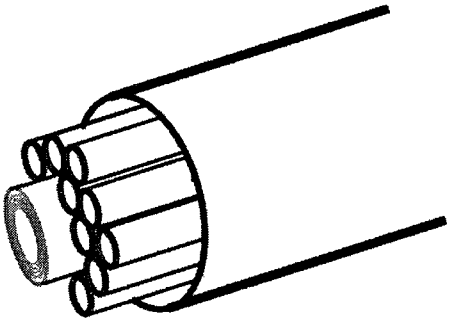

Figure 12: Schematic of a stacking process

Powder packing or solution casting methods were also attempted to make double core or porous fiber preforms. These novel mPOFs are made from biodegradable polymer materials, such as Cellulose and its derivatives and provide new application in medicine.

Finally, drawing of all the abovementioned preforms is investigated with an aim of producing long fibers of stable diameter and microstructure.

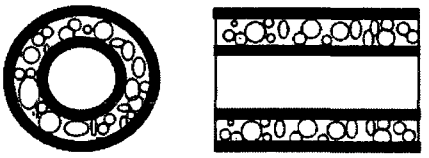

Figure 13: Schematic of a porous preform

0.4.4 Fiber drawing

Conventional single mode fiber is formed by pulling a solid glass preform into a geometrically similar fiber with $125\mu m$ diameter. The machine to enable such drawing is called the optical fiber draw tower within which furnace heats the preform to molten state then the preform is pulled into a thin fiber, as shown in Figure 14 (Freudenrich, 2007). The fiber is measured by a laser micrometer, and, finally the fiber is coated with a protective polymer jacket. In the end, the coated fiber is spooled on a take up device. The process control parameters are the furnace temperature, preform feeding speed and drawing speed (Keiser, 2000).

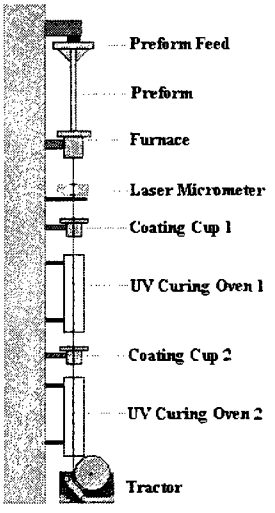

Figure 14: Schematic of a optical fiber draw tower

Microstructured optical fiber, however, requires more complex fabrication processes. One challenge is how to achieve the target hole size and shape during the

drawing. Holes can enlarge or shrink owing to the effects of surface tension, temperature gradients and pressure inside. Generally, researchers predict deformation by simulating the procedure of drawing and then deal with modifications in preform geometry design.

In the case of a polymer fiber, the preform can be drawn over a larger temperature range than glass fiber. During the draw process, the polymer chains are aligned, so that the final material is anisotropic along the fiber direction. Annealing after the draw can be used to relieve this internal stress (Eijkelenborg et al., 2001). When drawing multilayer Bragg fiber processing, parameters should be compatible with all the polymers. Moreover, one has to pay special attention to prevent distortion of a hollow microstructure by extensive shrinkage of expansion.

Chapter 1

Material Selection

In this chapter, selection of polymer materials for various fiber designs is in details.

1.1 Polymers for photonic crystal Bragg optical fibers

Due to the alternating layer structure of a Bragg fiber, two polymers used in Bragg fiber fabrication should have good optical properties at working wavelengths, and compatible chemical and rheological properties.

The sections II (Materials) and III (Solvents) in Appendix Article One: "Consecutive Solvent Evaporation and Co-Rolling Techniques for Polymer Multilayer Hollow Fiber Preform Fabrication" (Guo et al., 2006) detail the process of material and solvent selection. Two polymer materials should be optically, chemically, and thermodynamically compatible. We found that two polymer pairs - PMMA/PS and PC/PVDF as listed in Table 0.4.1 (Aldrich, 2006b) are the most suitable for the task.

The next mission is to choose low boiling point and non-toxic solvents for each polymer material. The solvents have to be "orthogonal" to each other so that they do not cross-solve the two polymers during a bilayer deposition. By using solubility parameters of polymers and solvents (Wypych, 2001) as a guide, for each polymer pair several solvent pairs were selected and tested in cross-solve experiments. The first step is solubility testing. Each polymer was tested to dissolve in its solvent in

Table 1.1: Polymer material pairs for Bragg optical fiber fabriaction

Material	T_g(℃)	Density(g/ml)	Refractive Index
PMMA	105	1.19	1.49
PS	100	1.05	1.59
PC	149	1.20	1.58
PVDF	-38	1.78	1.40

a glass test tube. After solubility was confirmed, the next step was orthogonality testing, the goal of which was to confirm that the solvents cannot dissolve the other polymer in pair.

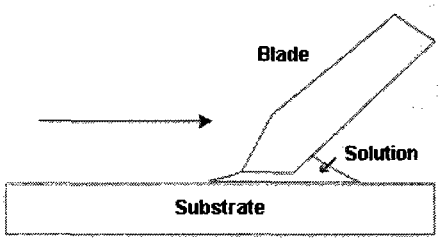

Figure 1.1: Schematic of the Doctor Blade technique

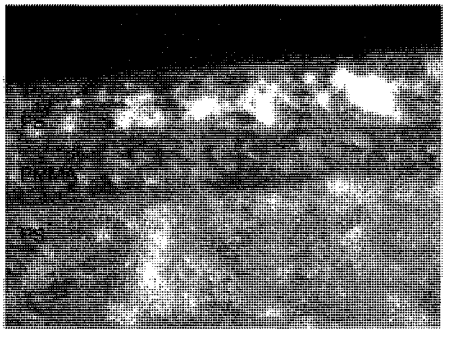

Figure 1.2: Interface of a 3 layers polymer multilayer film fabricated with Doctor Blade technique(PS/PMMA/PS)

Then, the Doctor Blade techniques was carried out to make multilayer films to test compatibility as shown in Figure 1.1. In this technique a small quantity of solution is dropped on the surface of glass slide and then wiped by a blade-like band. After

drying in an oven in a nitrogen environment, the next polymer layer was deposited on the former layer and the same procedure was repeated to form a multilayer structure. To analyse the interface, multilayer films were cut and the pictures were taken by an optical microscope. For example, from the image in Figure 1.2, we can see that the interfaces between PMMA/PS polymer layers are clear and easy to distinguish. This means that the solvent pair for PMMA and PS fulfills our requirements.

Table 1.2: Orthogonal solvents for the two pairs of polymer

Polymer	Solvent
PMMA	Acetone
PS	Cyclohexane+CCl_4
PC	Acetone or methyl acetate + $CHCl_3$
PVDF	CH_2Cl_2 or $CHCl_3$

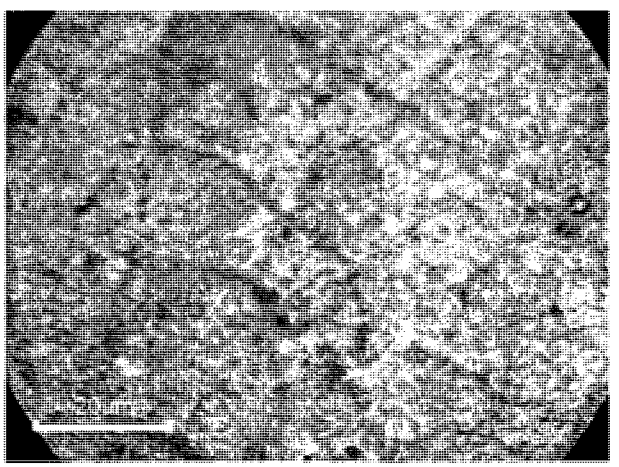

Figure 1.3: Micrograph of 3-layer polymer film (PS/PMMA/PS). Various imperfections on a surface are clearly visible.

When multilayer film surfaces were investigated under an optical microscope, small irregular stripes and cracks were visible across the film as shown in Figure 1.3. These stripes were the cracks in the layers. Particularly when a polymer solution touches the polymer film having residual stress during coating, cracks will appear and deteriorate the film structure. To solve this problem, annealing process is needed as post

treatment for every polymer film coating. Thus, after finishing drying of every new layer, the multilayer is heated to about 60°C, and held for about 3 hours to relieve stresses. Then the multilayer is slowly cooled down at a rate of about 5°C per hour to room temperature in the oven.

1.2 Polymers for biocompatible/biodegradable optical fibers

The polymers mentioned in former section above are not completely bio-friendly. A polymer based on the C-C backbone tends to be nonbiodegradable, whereas heteroatom-containing polymer backbones confer biodegradability. Biodegradability can therefore be engineered into polymers by judicious addition of chemical linkages such as anhydride, ester, or amide bonds, among others. The mechanism for degradation is hydrolysis or enzymatic cleavage resulting in scission of the polymer backbone. (Piskin, 1995)

A variety of natural, synthetic and biosynthetic polymers are bio- and environmentally degradable. Poly (esters) based on polylactide (PLA), polyglycolide (PGA), polycaprolactone(PCL) and their copolymers have been extensively employed as biomaterials. Other bio/environmentally degradable polymers include poly (hydroxyalkanoate) of the PHB-PHV class, additional poly(ester)s and natural polymer, such as cellulose and chitosan. (Dobrzynski et al., 1999)

The selection of biodegradable polymer materials for optical fiber fabrication is restricted by several factors just as that in the selection for Bragg fibers. There are low transmission loss, thermal stability, and good viscoelastic properties during drawing. Moreover, polymers with good solubility in regular non-toxic organic solvents will be better for the use in the casting film from polymer solutions for co-rolling preform manufacture techniques.

Based on these restrictions, PLA (Polylactic acid), PCL (polycaprolactone), CA (Cellulose Acetate), CB (Cellulose Butyrate) and HPC (hydroxypropyl cellulose) were

Table 1.3: Table of biocompatible/biodegradable polymer studied in the project

Material	T_g(°C)	T_m(°C)	Refractive Index
HPC	105		1.49
CB	100		1.59
CA	149		1.58
PLLA	-38		1.40

chosen in our work as biodegradable or biocompatible polymer materials for fabrication of waveguide fibers. The abovementioned polymers fall into two main group: synthetic polymers including polyester PLA and polylactone PCL; and derivatives of natural cellulose, CA, CB and HPC. Cellulose's derivatives form a family of cost-effective new materials via incorporating different chemical groups as substituents. In addition, various cellulose derivatives are widely available with various refractive indices, while offering similar thermal processing. The biodegradable materials we tested are listed in Table 1.2.

Chapter 2

Preform Fabrication Methodology

In this chapter, we detail various approaches that we used to fabricate mPOFs, including consecutive solvent evaporation, co-rolling, powder-packing and solvent casting techniques.

2.1 Consecutive solvent evaporation method

The section IV - "Multilayer Film Deposition Process" in Appendix Article One: "Consecutive Solvent Evaporation and Co-Rolling Techniques for Polymer Multilayer Hollow Fiber Preform Fabrication" (Guo et al., 2006) details the methodology of bilayer deposition for polymer Bragg fiber preform fabrication.

2.1.1 Deposition setup

Setup for consecutive solvent evaporation deposition, includes solution delivery system, and a rotation coater system. It was designed and manufactured by our research team (see Figure 2.1).

Figure 2.2 shows the image of rotation coater setup. Vibration free rotation around the axis of cladding tube is very important to the quality of the multilayer film. To reduce vibrations to low level, the whole setup is placed on top of a heavy desk and fixed tight with clamps. The rotation axis was aligned horizontally with great care. The cladding tube was fixed tightly on the frame by two end lids, additionally

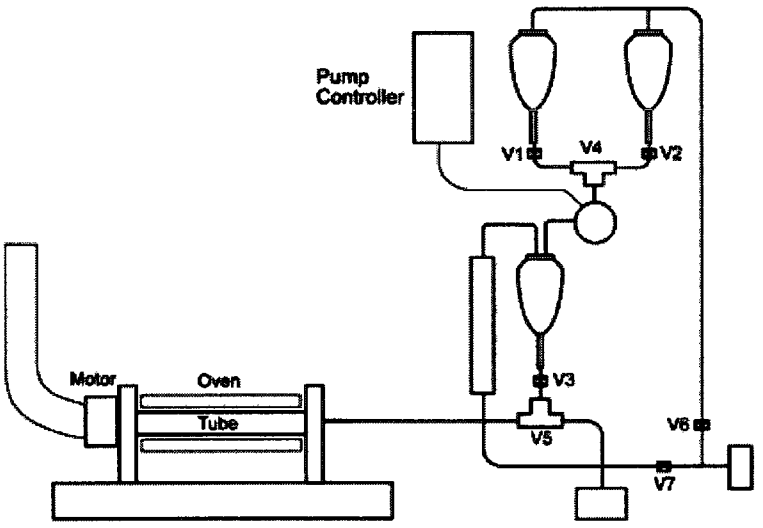

Figure 2.1: Schematic of a layer-by-layer deposition system. It consists of a rotation coater and delivery sub-systems

dumping vibration during rotation. Surrounding the cladding tube is the oven that allows to control temperature during coating process. The over is calibrated prior to multilayer depositing. We find that the temperature of a cladding tube and polymer solution during deposition is critical.

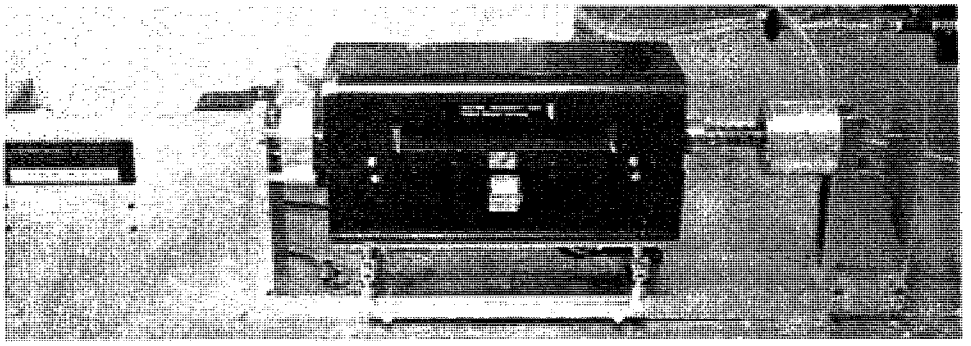

Figure 2.2: Image of a rotation coater sub-system

In the first experiments, the cladding tube was removed from rotation coater after deposition of every single layer, and filled with a polymer solution for the next deposition. In this case, the quantity of solution is not precisely dispensed. To overcome this problem, an automated delivery system was designed for delivering polymer solutions and pumping nitrogen gas with into the cladding tube as shown in

Figure 2.3. The entire unit was controlled with computerized valve switches.

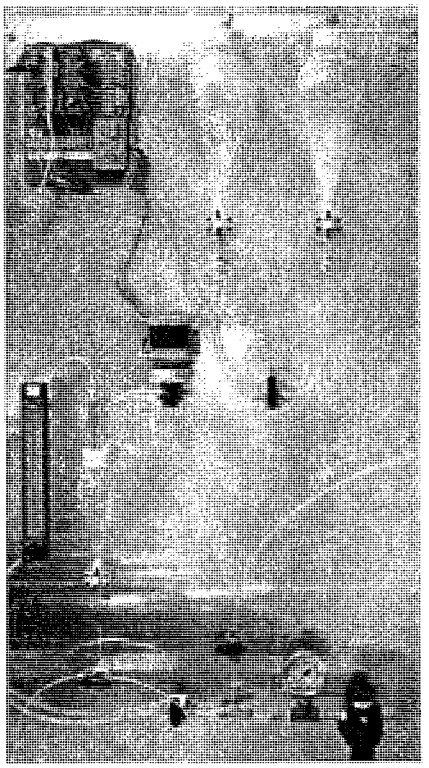

Figure 2.3: Image of Delivery System

2.1.2 Choice of substrate

Tube in the rotation-coater in Figure 2.2 serves as a substrate for the solution deposition. We tried glass tube at first as it offers many important advantages. The glass is a very stable material with standing the action of all solvents the used in our experiments. Smooth surface of a glass tube results in uniform films. In the coating process, the rotation speed could reach 3000Rpm and the glass is rigid enough to stand vibration of a tube. Glass is clear, so, it is easy to monitor the quality of the coating. When the deposition process is over, glass tube can be removed by hydrofluoric acid (HF).

However, in practice experiments, low adhesion between the glass tube and polymer multilayer became one serious problem. Before coating, glass tube was carefully

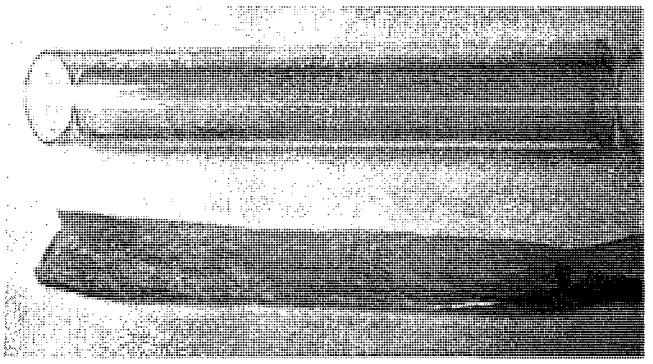

Figure 2.4: Polymer film peeled off from the glass tube. Choice of a cladding tubes is very important

washed with soap and acetone to eliminate impurity like dust and grease on the surface. The first layer film deposition is usually of good quality - smooth surface and uniform thickness. Once the second layer is coated, the entire polymer film peels off from glass, as shown in Figure 2.4. The major reason is a large difference in thermal expansion coefficients between glass and polymers and low adhesion between materials. For example, in Table 2.1.2, we compare the typical thermal expansion coefficient of several materials. The coefficient of thermal expansion of polymer is 100 times large than that of silica glass. When a glass tube and a polymer film were heated and cooled down continually during the coating process, stresses at the interface caused the separation of a polymer film from tube.

Table 2.1: Comparison of thermal expansion coefficient for different cladding materials

Material	Coefficient of thermal enpension $\alpha(10^{-6}/K)$
Silica	0.4
Steel	12
Polystyrene	90-150
Teflon	126-216

We then investigated polymer cladding tubes a alternative deposition substrate. Using polymer tube has one highlight advantage, which is that it is not necessary

to remove it from the end of preform. After the deposition process, the polymer tube becomes a part of a cladding and it enhances the mechanical property of the preform. For the PMMA/PS and PVDF/PC combinations, PMMA and PC cladding tubes were chosen respectively. Since the cladding tube and multilayer film are all polymers, the coefficients of thermal expansion are similar and adhesion compatibility is much better compared to a glass/polymer system.

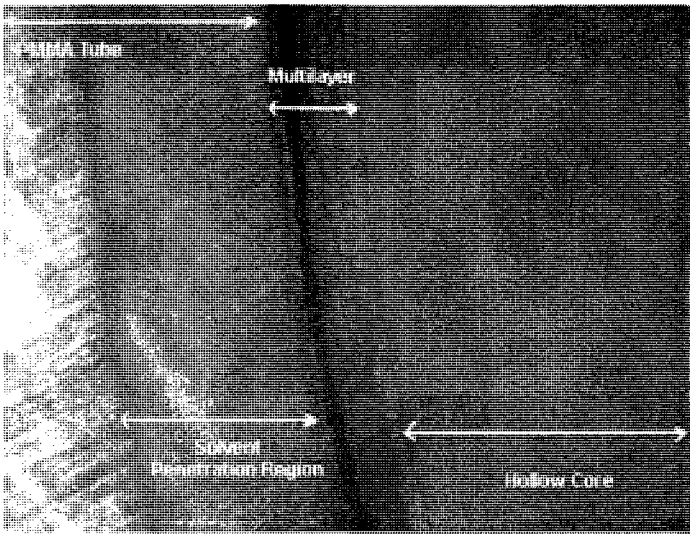

Figure 2.5: Polymer cladding tube. Structure of the interface between cladding tube and polymer multilayer

With a polymer tube, however, the problem arises due to solvent penetration into the cladding tube. As shown in Figure 2.5, during multilayer deposition the solvent was not only taken away by evaporation, but it also diffused into the polymer cladding tube during deposition process. Solvent diffusion depth depends on solvent, heating temperature, and revolution speed. This residual solvent is a prime reason for the bubbles formation during fiber drawing, we will discuss detail in next chapter.

During the first experiments, we have also observed cracks inside of the cladding tube during the deposition process (see in Figure 2.6). This phenomenon is quite similar to what happens in multilayer coating experiments by the Doctor Blade technique. The PMMA cladding tube we used is made by extruded acrylic from McMaster-Carr

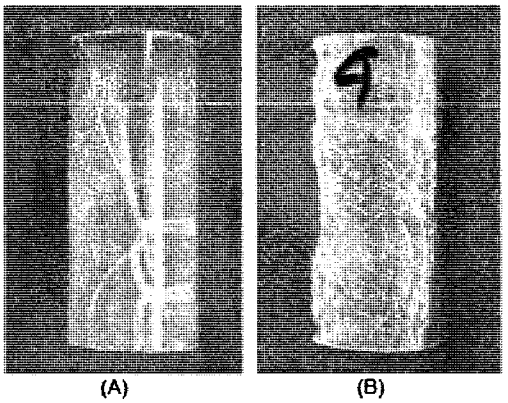

Figure 2.6: Pretreatment of polymer cladding tube is critical for the quality o f resulting preform. Cracks in the non-treatment tubes. (A)PC tube; (B)PMMA tube

Company. Therefore, residual stress promotes tube cracking when polymer solution contacts the surface of tube. Annealing technique was carried out to solve this problem. Each tube was put into oven after be completely cleared with soap and ethanol. Then the oven temperature was increased to about 90°C, which is lower than polymer's $T(g)$ to avoid deformation, for at least 6 hours to release residual stress. In the next step, the temperature was reduced gradually at a rate of 5 degree/hour. This approach solved the problem of tube cracking.

2.1.3 Deposition process

The quantity of polymer solution injected into the cladding tube depends on the desired film thickness at the range (typically of 20 to 100μm). The rotation speed is from 1000 to 2000 Rpm when the solvent is evaporating. For a given polymer solvent pair, coating conditions such as nitrogen flow velocity, rotation velocity of a tube, and solution concentration, must be optimized to increase quality of the deposited films. Details for PMMA/PS and PVDF/PC pairs presented in the section IV (Multilayer film deposition process) of Appendix Article One: "Consecutive Solvent Evaporation and Co-Rolling Techniques for Polymer Multilayer Hollow Fiber Preform Fabrication" (Guo et al., 2006).

2.2 Co-rolling method

An alternative technique for the Bragg fiber preform is a co-rolling method. In this method, several different polymer films were co-rolled around a mandrel to form either solid core or hollow core preforms. The main disadvantage of this method is that it is impossible to vary the thicknesses and compositions of individual layers. Using this method, we demonstrated 32 layer preforms of PS/PMMA and PC/PVDF combinations. Section IV (Preform fabrication by co-rolling of polymer films) in Appendix Article One: "Consecutive Solvent Evaporation and Co-Rolling Techniques for Polymer Multilayer Hollow Fiber Preform Fabrication" (Guo et al., 2006) details application of this method.

2.3 Powder packing and solution casting methods

We developed the techniques to fabricate biodegradable fiber preforms. We started with a description of a powder packing method in a double core fiber design. Two sizes of CB tubes were used to create two core. The inner 1/8inch inside diameter and 1/4inch outside diameter; and the outer one had the inside diameter of 3/8inch" and outside diameter of 5/8inch. The space between two tubes was packed with HPC powder. The small tube packed was sealed at both ends to prevent from HPC powder getting into the core. The HPC powder was filled in the space between the two tubes in several batches. After each batch of filling, light force was used to knock the tube in order to promote tight and uniform packing of the powder. When the powder was filled, the inner tube's space was sealed with Teflon tape. Final preform fabricated this way is shown in Figure 2.7(A). Two HPC powders of different molecular average $M_w \sim 370,000$ and $M_w \sim 80,000$ were tested.

During the drawing process, we sometimes observed collapse of the outer tube onto the inner one due to non-uniform distribution of HPC particles along the fiber length. To improve this situation we developed a solution casting method to fill the

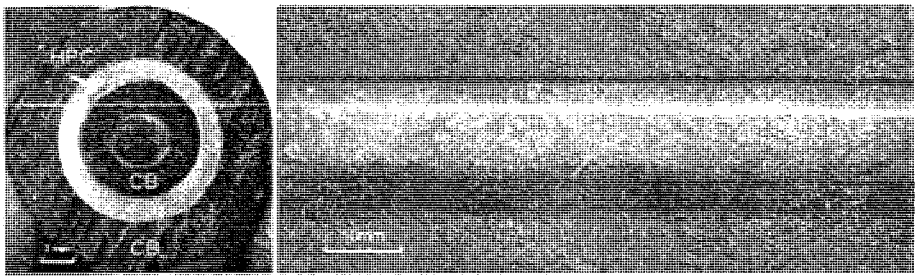

Figure 2.7: Images of biodegradable fiber preform. (A)cross-section of all-cellulose preform fabricated by powder packing; (B)all-cellulose preform by solution casting

inner tube space with HPC. Particularly, we took advantage of solubility of HPC in water at ambient temperature. HPC in a solution of water was filled in the gap between CB tubes and the water was then evaporated in vacuum oven. The preform is shown in Figure2.7(B).

Chapter 3

Fiber Drawing

3.1 Introduction

Due to complexity of the microstructured polymer optical fiber (mPOF), the fabrication of mPOF is more difficult compared to the traditional polymer optical fibers(POF). In this chapter, we details drawing processes of all-polymer Bragg fibers.

3.2 Draw process and draw tower

We start by describing the basic principles of fiber drawing. During drawing, the preform is positioned vertically in the center of the vertical furnace. When the temperature of the preform is rased above its softening point, the lower end of the preform necks downward by gravity. Then, additional tension is applied to the fiber by a tractor and the fiber is pulled down continuously while the preform is fed at a certain rate into the furnace.

Draw Tower

Figure (3.1) shows the image of a draw tower in our laboratory. The tower consists of several major parts: cleanroom enclosure preform holder and downfeed axis, two zone furnace, laser micrometer, tractor, spooler drive, preform pressurization assembly, etc. The machine is about 6 meters of height and can draw fibers to $100\mu m$.

On the top of tower, a clean-room enclosure hosts furnace, preform feed assembly,

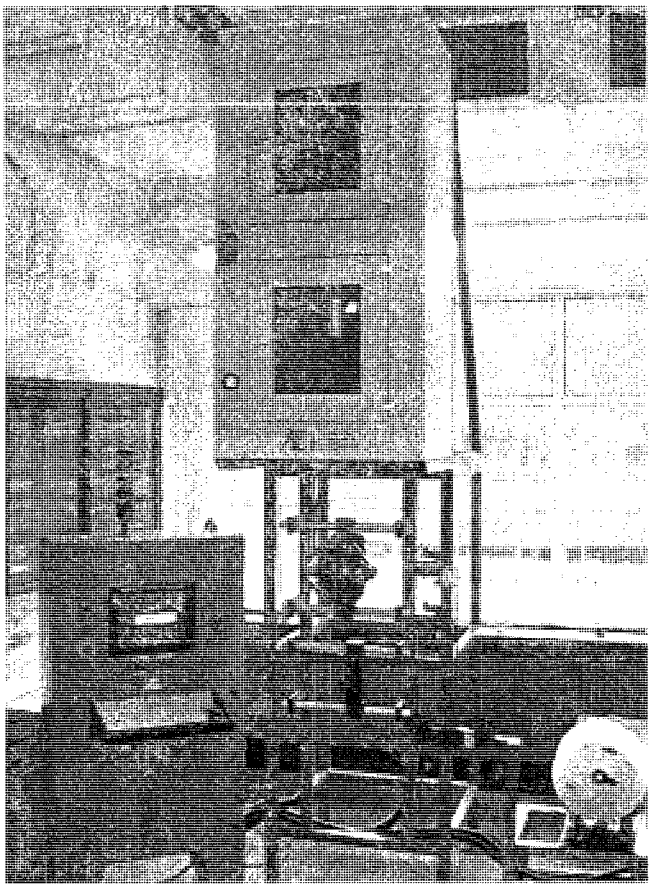

Figure 3.1: Image of polymer optical fiber draw tower in our laboratory

and laser micrometer and provides clean environment the drawing processing. The preform feed assemble is to regulate the feed rate of preforms into the furnace. The feed speeds it can provide are in the range of $0.025mm/min$ and $30mm/min$. The downfeed axis has approximately 430mm of vertical travel, thus allows preforms of $380mm$ long. The preform holder has three adapters to accommodate preform with $30mm$ outer diameter.

Two stage furnace is the critical part of a draw tower. In the furnace the preform is heated and tapered into the fiber. Our 2-zone furnace features a quartz liner. Each of two heat zones is $150mm$ long and is independently controlled by an intelligent PID (P-Proportional, I-Integral, D-Derivative) temperature controller with feedback form a type K thermocouple (Omega HH501D). The maximum temperature that

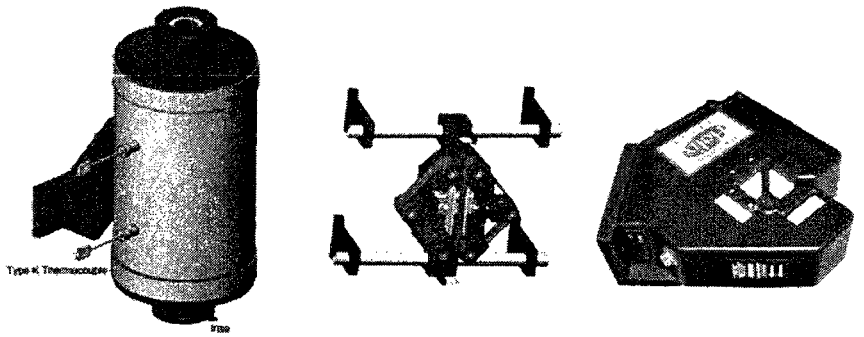

Figure 3.2: Components of a draw tower. (a)2 zone oven; (b)tractor; (c)laser micrometer

furnace can reach is about 1000°C (AEI, 2005), which cover the melting temperature of polymers and most of soft glass. Prior to running the draw tower, the furnace is profiled to understand the non-uniformities in temperature distribution.

After preform is tapered into fiber and drawn outside of furnace, the fiber diameter is monitored by a laser-based diameter gauge (Holix 500 from Beta LaserMike Company). This laser micrometer is located directly below the furnace and measures continually the fiber diameter during the draw processing. It then transfers the results to the feedback PID system to adjust draw parameters in order to maintain constant fiber diameter. Both X and Y dimension can be measured in the range of 0.038 to 6.4mm of outer diameter at 490Hz scan frequency (AEI, 2005).

The tractor, which is responsible for pulling the fiber out of the furnace at set speed, controls the squeezing pressure and pulling speed. Drawn fiber is finally collected by wspooling it onto a bobbin. rapping them onto a spool. Drawing spooling is controlled to ensure proper long-term storage.

3.2.1 Drawing procedure and parameters

Typically, the drawing process consists of a two steps. The first step is preform preheating. The preform is aligned along the axis of a cylindrical furnace and then heated somewhat over its Tg of preform materials. The preform is then kept in a furnace

for several hour for all over temperature equalization inside of the furnace. The time for temperature stabilization differs depending on materials, preform structure, and other environment factors. In general, the longer time the preheat process takes, the better temperature equalization will be. However, in the case of a microstructured preform, too long of a preheat time will increase the risk of structure collapse. In the next step, the temperature of the oven is raised to a drawing point, which is maintained throughout the whole drawing process. Then, the preform is fed at a constant velocity into furnace where it necks down to the final diameter due to an applied draw force by the tractor.

There are several critical parameters that affect resultant fiber diameter and quality, among which, drawing temperature and draw speed are the most important. Only certain restricted combinations of furnace temperature and draw speed result in good fiber, especially in the case of mPOFs. The furnace temperature distribution, preform feed velocity and pressurization are other important parameters, which affect the quality of the fibers.

In particular, during Bragg fiber drawing, hollow core collapse due to surface tension effects the uniformity of a photonic crystal reflector in the resultant fiber as well as fiber optical properties. There are two parameters, a drawdown ratio and a core collapse ratio, that describe completely all the geometries of a resultant fiber. Defining R_i^f and R_o^f to be the inside and outside radii of a hollow Bragg fiber, while R_i^p and R_o^p to be the corresponding radii of a preform, a drawdown ratio D, defined as $D = R_o^p/R_o^f$, relates the preform and fiber outer diameter. Core collapse ratio C_r, defined as $Cr = (R_o^p/R_o^f)/(R_i^p/R_i^f)$, and it characterizes core collapse in a fiber compared to preform. Drawdown ratio is typically set before drawing and can be maintained directly by the feedback loop. As for C_r, it cannot be controlled directly. When $C_r = 0$, the core collapse is complete resulting in a solid core Bragg fiber; while $C_r = 1$ means that there is no core collapse at all, with the same drawdown ratio characterizing reduction of both outer and inter diameter are equal.

The C_r as close to 1 as possible is desirable drawing fabrication of hollow Bragg fibers. In the simulation models conducted in our group, the collapse ratio is modeled as a function of drawing temperature, drawing speed, feeding speed and draw ratio (Pone et al., 2006). The main conclusion are as follow. The effect of the drawing temperature is that the viscosity of polymer decreases rapidly with the reduction of the temperature, thus hindering the hole collapse. The drawing speed's effect is also easy to understand. Increasing the drawing speed reduces the collapse due to the shorter time the fiber spends in the melted zone, hence a lesser effect of a surface tension.

$$D_n = \frac{V_{drawing}}{V_{feeding}} = \frac{S_{preform}}{S_{fiber}} \tag{3.1}$$

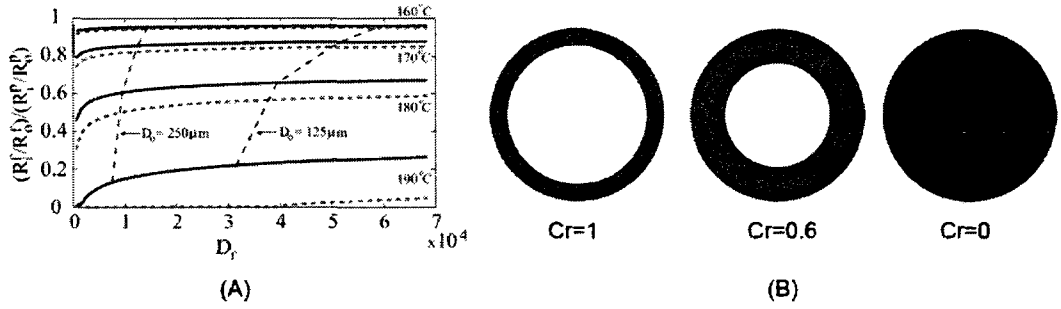

Figure 3.3: (A)C_r as a functional of draw ratio D_r, solid line correspond to multilayer preform, dotted lines correspond to a simple tube with the same thickness as multilayer preform, dashed lines represent the curves of a constant outer diameter. (B)schematic shapes of hole collapse while C_r=1,0.6,0

3.3 Microstructured preform drawing

In this section,drawing of Bragg fibers, composed of PMMA, PS, PVDF and PC polymers is detailed including successful and un-successful experiments.

3.3.1 Drawing of capillaries from a pure PMMA tube

The first drawn samples were the PMMA tubes, with outer diameter were in the range from $1.25inch(31.75mm)$ to $1inch(25.4mm)$; and wall thickness in the range of

$0.25inch(6.35mm)$ to $0.125inch(3.175mm)$. All these tubes were from McMaster-Car Company (http://www.mcmaster.com) and were made by the extrusion technique. The Drawing of PMMA tube provided us with the important information on PMMA thermomechanical properties. Furthermore, drawing of tubes was a natural starting point to study the basic effects of drawing parameters on the core collapse of resultant capillaries.

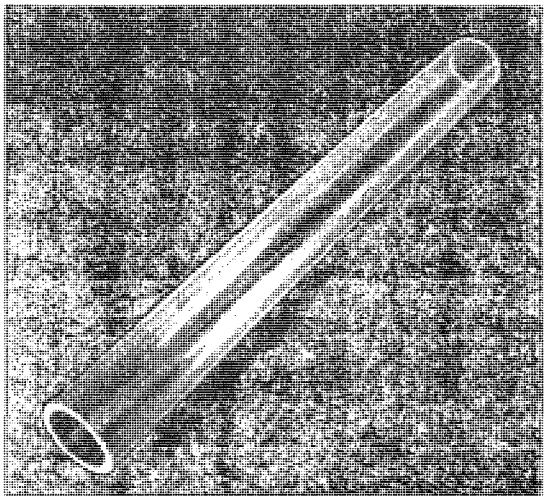

Figure 3.4: Image of a PMMA tube. The OD is 31.75mm, the wall thickness is 6.35mm and the length is 450mm

Processing details are as follow. First, a PMMA tube was cut to $450mm$ to fit the furnace. Then, it was cleaned with distilled water and degreased with ethanol. After been dried, four small holes were drilled at one end of the tube to attach the bait weight, which was used to aid necking down at the beginning of drawing. Finally, the preform was loaded into the holder and placed into furnace.

We found that degassing and annealing of tube should processed before the drawing, as a commercial PMMA tubes are not pre-processed for drawing. For example, during the PMMA synthesis process, there are small amounts of residual monomer present in the final product (Ohe et al., 1989), as well as some trapped gas and solvent. Initially, the residual monomers, gas and solvent are not visible and are diffused through the polymer matrix. When the tube is heated, trapped gases and solvents

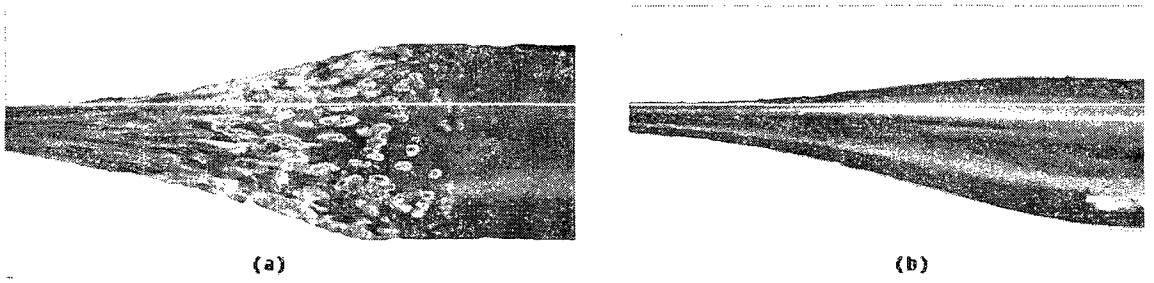

Figure 3.5: Images of a neck-down zone of a PMMA tube. (a)when drawing without degassing, many bubbles were in the tapered region. (b)when degassed, there were no bubbles

expand in size and till the bubbles bigger are forward enough to be see by naked eyes, as shown in Figure 3.5. During drawing, bubbles stretch out and result in reduced strength, line defects, diameter non-uniformity.

By heating the tube below the material T_g, which, in turn, is lower than drawing temperature, the diffusion of gases and solvents can be provided, and they gradually escape from the preform. This is called degassing. Higher temperatures reduce degassing fine, however, the tube is easy to deform at temperatures close to T_g. To reduce degassing time and prevent tube deformation, we found that for PMMA, $T = 100$°C was optimal. In Figure 3.5(b) drawing of a degassed tube us shown. Only a few bubbles in PMMA tube were visible after baking the tube for 2 hours at 90°C.

Table 3.1: Typical drawing parameters for PMMA tube

Drawing Parameter	Value
Preheat Temperature (°C)	130
Preheat Time (Minutes)	120
Oven 1 Drawing Temperature (°C)	170
Oven 2 Drawing Temperature (°C)	170
Fiber Diameter Setting (μm)	500

Table 3.3.1 shows the typical drawing recipes for Acrylic (PMMA) tube. Control of the fiber drawing process is based on a PID algorithm, which accounts for 3 major

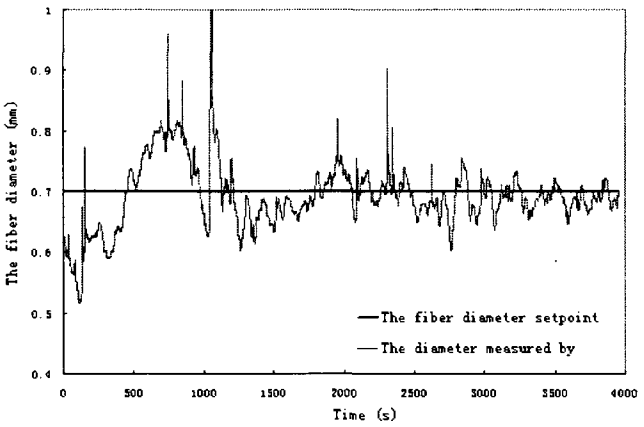

Figure 3.6: Fiber diameter fluctuation during drawing process

factors of a linear system. The P-term represents a proportionality constant by which a modification is applied to the current state of linear system. The I-term represents an integrated term that controls a linear system long-term stability around the setting point. And The D-term represents a differential modifier to the current state. The drawing process of mPOF, however, is not a linear system due to inherent non-uniformity of a polymer preform variations in the oven temperature distribution and other noise factors. However, the PID control loop can still control a fiber drawing process well assuming that time variation of control parameters are small. As shown in Figure 3.6, the fiber diameter tended to the set point after draw begin in a period time of about 7 minutes when the values of PID were set to $P = 8\%, I = 0\%, D = 40\%$ respectively.

We then studied core collapse of a capillary as a fuction of drawing speed. Thus one PMMA tube was drawn at three different speeds (2000, 3000, 4000mm/min) with other parameters kept constant. The resultant fibers were cut and the cross-section were photographed and analyzed.

Figure 3.7 shows the cross-section of these fibers and fitted images. In Table 3.3.1, the results of draw ratio and collapse ratio are presented. From the data, we can conclude that for the large diameter fibers of 700um, hollow core collapse is

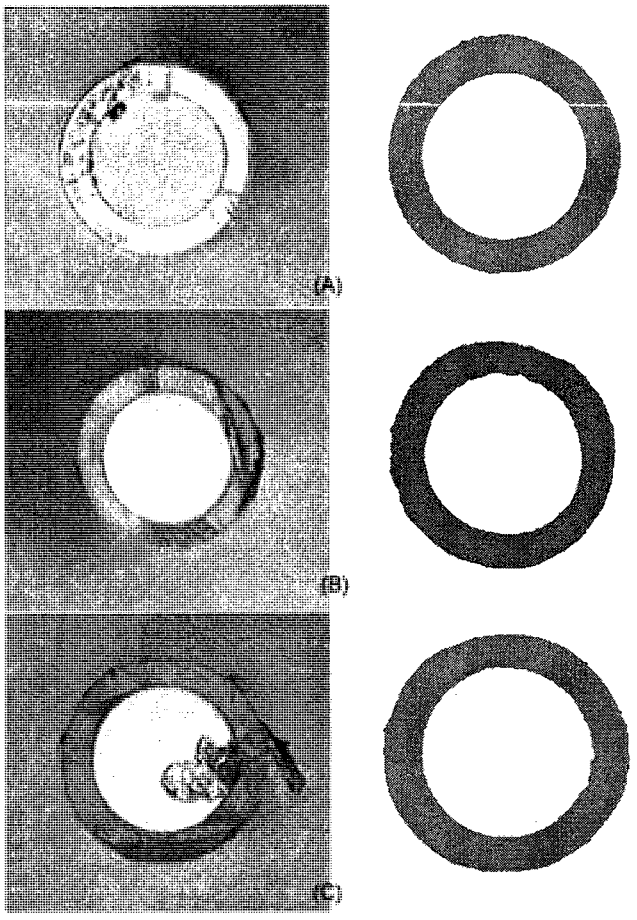

Figure 3.7: The cross-sections and fitted images of fibers drawn at draw different speeds (Vd). (A)$2100 - 2300(mm/min)$; (B)$3200 - 3400(mm/min)$; (C)$4000 - 4300(mm/min)$

small 0.95 and doesn't depend strongly on the draw velocity. Our further experiments showed that core collapse in smaller diameter fibers is considerably more pronounced.

3.3.2 Drawing of Bragg fibers from the preform made by solvent evaporation coating method

As detailed in Chapter 2, we developed a new technique to manufacture a Bragg multilayered preforms by solution coating. For the PMMA and PS combination, the maximum number of transparent and well attached layers demonstrated was 20. Figure 3.8 shows the schematic and a real cross-section images of a Bragg fiber preform with 10 layers.

Table 3.2: Summary of draw ratio and collapse ratio for selected fiber samples

Drawing parameter	Fiber 1	Fiber 2	Fiber 3
Drawing speed (mm/min)	2100 – 2300	3200-3400	4000-4300
Preform outer diameter (mm)	25.4	25.4	25.4
Preform inner diameter (mm)	18.8	18.8	18.8
Mean fiber outer diameter (μm)	202.31	196.88	199.17
Mean fiber inner diameter (μm)	141.61	137.18	138.88
Mean fiber diameter mean ratio	0.7000	0.6968	0.6973
Drawdown Ratio	125.7	129.0	127.5
Collapse Ratio	0.9457	0.9414	0.9420

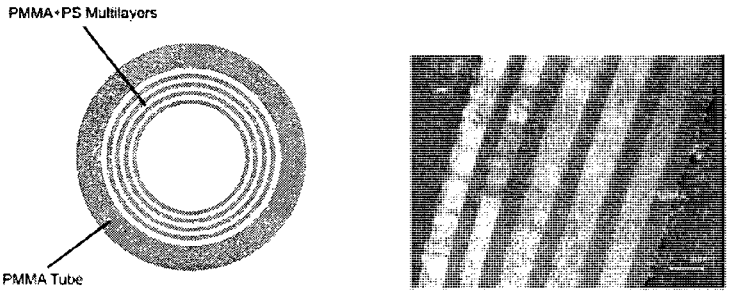

Figure 3.8: Schematic and cross-section images of a Bragg fiber fabricated by solvent evaporation method. The number of multilayer is 10

Unfortunately, this nice looking didn't result in a good fiber. More precisely, when the preform was heated over 80°C, bubbles emerged and further expanded as the temperature increased. Finally, the bubbles covered the whole surface of the inside of the preform as Figure 3.9.

From the primary analysis, we concluded that this due to the residual solvent trapped into the cladding tube during preform fabrication. Normally, Gas Chromatography (GS) method is used to observe the residual solvent in polymer. However, we carried out a simple method - weight-loss experiment to monitor the remaining solvent in a preform. In the experiment, multilayered preform was placed into a vacuum oven to degas solvent (see Figure3.10). The preform was weighted every day, and the weight loss was attributed to the degassed solvent.

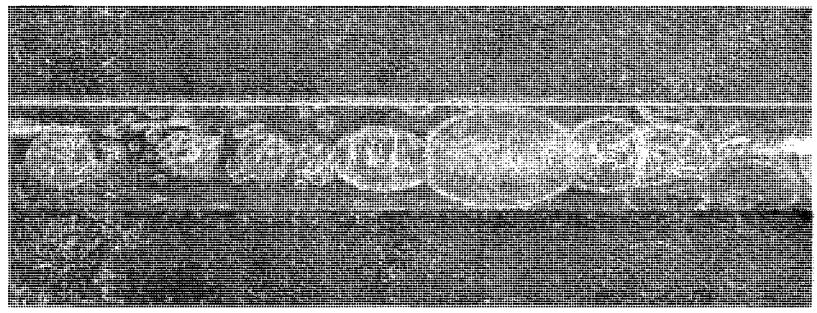

Figure 3.9: Due to imperfect solvent trapped in preform, bubbles appeared during drawing

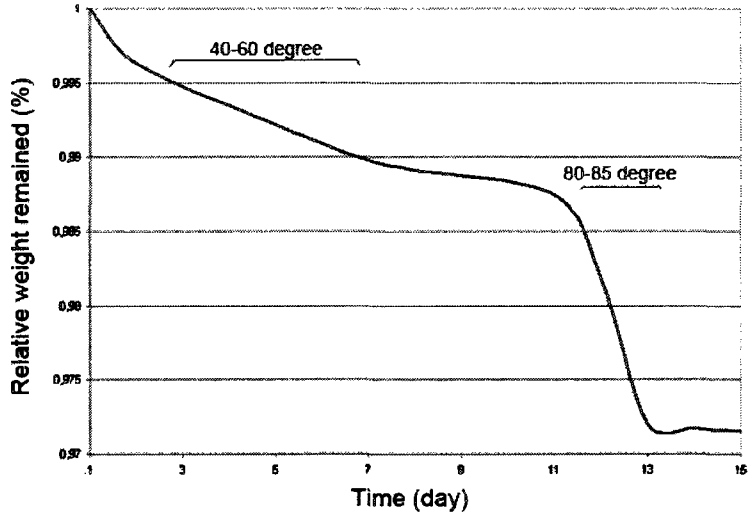

Figure 3.10: Preform weight Loss in solvent extraction experiment

There are two temperature regions where preform weight drops quickly. One region is for temperature around 60°C, while the other one for temperature around 85°C. These temperature correspond to the boiling point of solvent used in preform fabrication. Cyclohexane and acetone have boiling point of 81°C and 56°C respectively (Aldrich, 2006a). Therefore, we can draw the conclusion that the weight loss in two temperature regions is due to the evaporation of two solvents when the temperature is close to their boiling point. Acetone has the lower boiling point, and therefore it is easy to be vaporized during the coating process. So we mostly focused on how to eliminate residual cyclohexane. Following each layer coating of PS, the preform was placed into the oven for baking 80°C over boiling temperature of cyclohexane. After

this additional process, the preform needed to be annealed again for the next layer coating, thus slowing the preform fabrication process.

The preform made by the modified coating method was drawn again. The bubbles formation was suppressed completely below 100℃ compared to that of a former preform. Nevertheless, when the temperature got higher than 100℃ bubbles appeared again. This temperature was much higher than both boiling points of the two solvents, so the nature of the is still investigation. Figure 3.11 shows the preform full of bubbles and the cross-section of a resultant fiber. This bubbling phenomena occurred not only in the case of PMMA/PS combination, but also in the case of PCDF/PC combination. The further experiments are in progress to understand this phenomena.

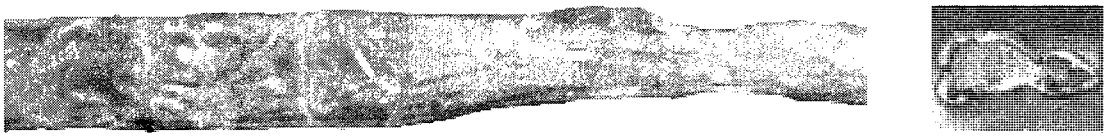

Figure 3.11: Drawing Bragg fiber preform fabrication by solvent evaporation

3.3.3 Drawing of Bragg fibers from the preform made by co-rolling method

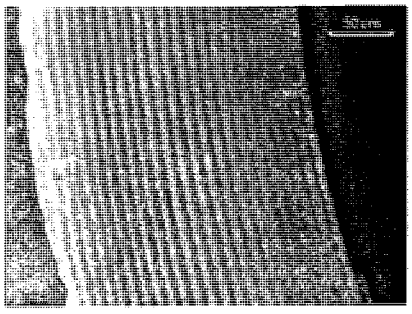

Figure 3.12: The cross-section of PMMA/PS Bragg. The fiber diameter is 250um

For the Bragg fiber preforms made by co-rolling method, we didn't encountered the bubbles problem after the films degassing process. Stable diameter Bragg fiber can be drawn from such preform (see Figure3.12). Drawing temperature of PMMA/PS

Bragg fiber was different from the drawing temperature of pure PMMA or PS tubes. In fact, PS reveals a difference behavior from PMMA during drawing. Though PMMA and PS have similar (T_g)s, which are 100°C and 95°C respectively, the optimal drawing temperatures are quite different. From the experiments, the temperature for drawing pure PMMA preform is about 170°C and the temperature for drawing pure PS is about 210°C. When PMMA and PS are co-rolling together, the drawing temperature is in-between the two drawing temperatures of the pure materials. Table 3.3.3 shows three different drawing temperatures from low to high - for drawing pure PMMA tube, Bragg preform with equal thickness of PMMA and PS, and pure PS tube preform. We conclude that more PS material in a preform lead to higher drawing temperatures.

Table 3.3: Fiber drawing temperatures for preforms with different ratios of PMMA and PS polymer

Type of Preform	Drawing temperature (°C)
Pure PMMA Tube	170
Bragg PMMA and PS Preform	190
Pure PS Tube	210

We have also used drawings in attempt to increase the resultant draw down ratio. Higher draw ratios result in thinner layers hence shorter wavelength of operation. Thus, after the first drawing, a piece of fiber was inserted into a cladding rod, featuring a drilled hole and then the drawing process was repeated. Figure 3.13 shows the cross-section of a final polymer optical fiber with $1mm$ outside diameter and $20\mu m$ inner diameter. The total draw ratio was about 1250, which is much larger than the drawdown ratio that can be achieved in one-step drawing process.

For the co-rolled Bragg fiber preform with PVDF/PC material combination, the drawing process was essentially the same as for PMMA/PS material combination. Compared with other fluoropolymers, drawing PVDF was easier because of the PVDF

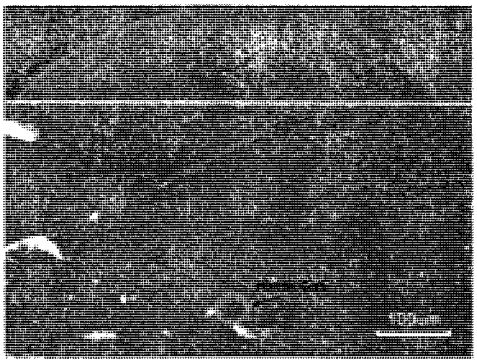

Figure 3.13: The cross-section of a Bragg fiber drawn by two-step technique

relatively low melting point. Polycarbonate (PC) also had good thermoplastic properties similar to these of PMMA. A typically PVDF/PC fiber cross-section is shown in Figure 3.14.

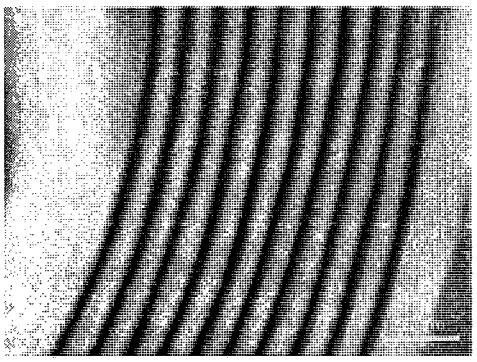

Figure 3.14: Cross-section of PVDF/PC Bragg fiber

Chapter 4

Biodegradable Microstructured Fibers Drawing and Characterization

Although PMMA and PS plastic are biofriendly, which means these materials have no toxic or injurious effects on biological systems, but there are not however fully biocompatible. We have attempted to develope several kinds of biocompatible fibers basing on polylactide(PLA), polylacticacid(PCL), and cellulose derivatives in a view of bi-medical applications. In this chapter, the biocompatible fiber drawing processes and its optical properties are introduced.

4.1 Polymer fiber made with PLA/CA material combination

One type of biodegradable Bragg fiber preform was made of PLA and Cellulose Acetate(CA) by film co-rolling method. PLA/CA combination has good thermal compatibility as semi-crystalline PLA has a melting temperature of 152°C and amorphous CA has a glass transition temperature of 150°C. Step index PLA/CA preform was thus fabricated. PLA film of 100 micron thickness was manufactured in-house while CA film of 125 microns thickness was obtained from MacMaster Canada. After co-rolling around the mandrel of 20 centimeter diameter, the preform was solidified at

170℃ in vacuum oven for about 10 minutes.

The preform, as shown in Figure 4.1, was about 25 centimeter of length and in good quality - clear, transparent, uniform and smooth surface. After it was pre-heated at 150℃ for 1 hour, the temperature was increased up to 225℃. As a result, Smooth, uniform and transparent fibers with diameters range from 400 to 1000μm were obtained. The cross-section of fiber is shown in Figure 4.1. The color of the fiber however turned yellow, which indicates that some degradation took place during the drawing process. Moreover, thickness of the core layer is quite nonuniform due to imperfect home-made PLA films. Finally, the fiber is stiff and brittle at room temperature.

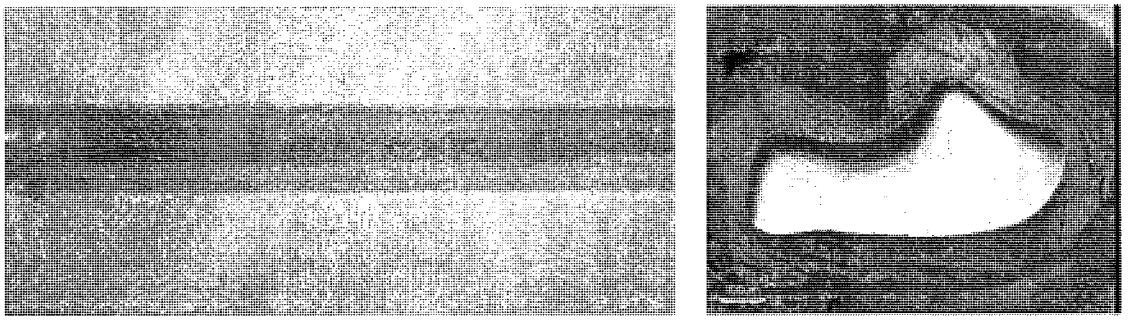

Figure 4.1: Biodegradable PLA/CA preform and cross-section of fiber

4.2 Biodegradable cellulose-based microstructured fiber

We designed and fabricated several types of microstructured fiber preforms, based on cellulose derivatives only. One practical examples is a double-core porous structure as introduced in chapter 3. We used cellulose butyrate(CB) and hydroxypropyl cellulose(HPC) material combination. These materials are completely biocompatible and even biodegradable under natural conditions.

Prior to microstructured preform drawing, a single CB tube was tested to obtain optimized drawing parameters. The CB tube showed good thermoelastic properties

Table 4.1: Drawing parameters for pure cellulose butyrate (CB) tube

Drawing Parameter	Value
Preform Material	Cellulose Butyrate (CB)
Preform Outer Diameter (mm)	16
Preform Length (mm)	300
Preheat Temperature (°C)	130
Preheat Time (Minutes)	60
Drawing Temperature (°C)	178
Fiber Diameter Setting (μm)	500

comparable to those of PMMA. When drawing temperature was lower than 175°C, fiber drawing became difficult and the obtained fibers were milky; when the drawing temperature was higher than 184°C, CB showed high fluidity and draw uncontrollably. The proper drawing temperature was limited to the narrow range from 175 to 184°C. Table 4.2 shows typical parameters for CB tube drawing.

Porous double-core polymer optical fiber

Hydroxypropyl cellulose(HPC) is one of the cellulose derivatives with glass transition temperature of 100°C compared to 120°C of CB. Double-core microstructured CB preforms with Hydroxypropyl Cellulose (HPC) filling in space between the two core with parameters similar to draw parameter in Table4.2.

Initially, the preform was packed with high molecular weight HPC $M_w \sim 370,000$. Although we obtained some fiber, however, the polymer particles stuck to each other and the fiber diameter varied greatly (see Figure4.2).

One solution was to decrease molecular weight of HPC and thereby to reduce its viscosity and to improve its fluidity during fiber drawing process. In the following experiments, HPC powder of smaller $M_w \sim 80,000$ molecular weight was used to fill the space between the two cores. Several experiments were carried out to investigate melting of HPC powder and CB tube. A piece of CB tube and some amount of HPC

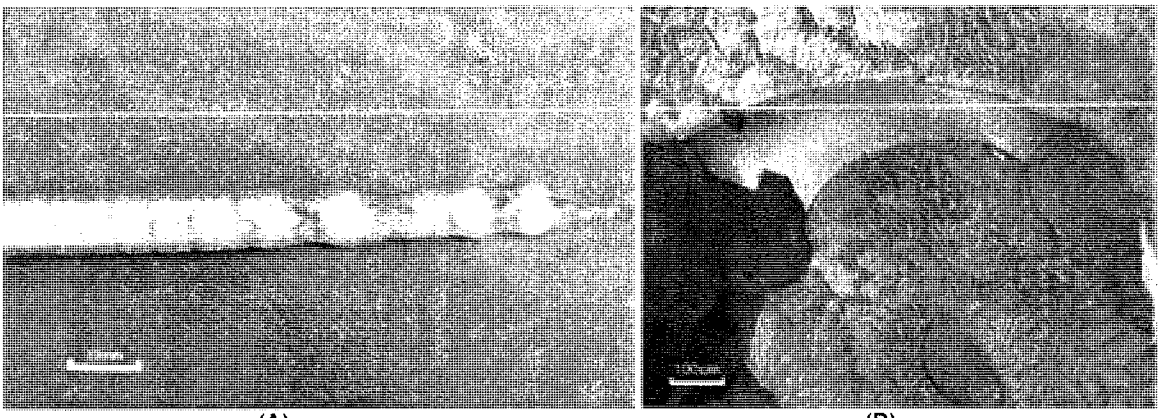

Figure 4.2: Double-core fiber packed with high molecular weight($M_w \sim 370,000$) HPC powder. (A)Tapered preform; (B) The Cross-section of fiber.

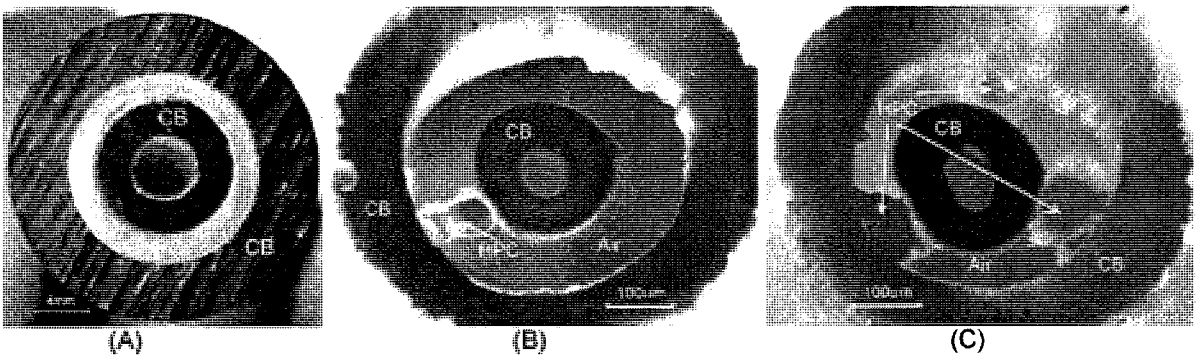

Figure 4.3: Images of fiber fabricated by powder packed with lower molecular weight HPC powder $M_w \sim 80,000$. (A)Cross-section of porous double-core preform; (B) and (C)fiber cross-section.

powder were loaded in a petri dish into a oven. Samples were heated in an oven at 90, 130, 170℃, and 180℃ respectively for a couple of hours each time. It was found that at 130℃, CB tube started to soften; however HPC powder remained unchanged. At 170 and 180℃ CB tube soften considerable, while HPC powder only partially melted.

Basing on these initial experiments we processed with preform fabrication. After solidification in oven at 115℃ for about 2 hours, the porous double-core structured preform, as shown in Figure 4.3(A), was drawn again with the same parameters as in the initial experiment. This biodegradable fiber was drawn down to a diameter of

$450\mu m$. From the study of fiber cross-section (Figure4.3(A) and (B)), it is clear that the smaller inner core is suspended in air by the low refractive-index and water-soluble particles (HPC), seperating it from the outer core. This type of geometry has many potential applications to laser power delivery, reflect light collection, microfluidics and drug's release for bio-medical application.

Polymer fiber of PCL and CB combination

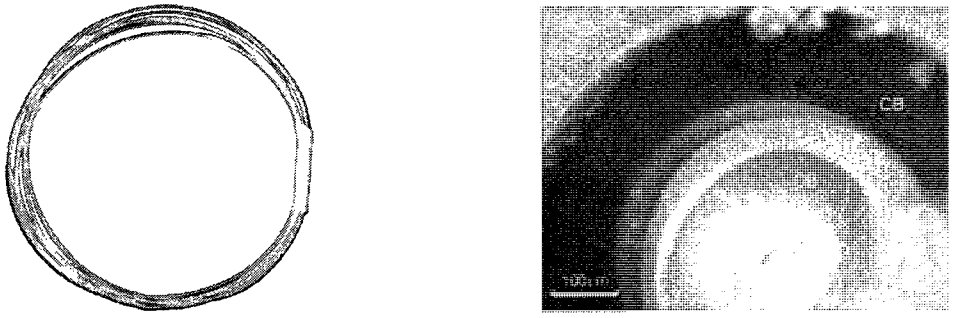

(A) **(B)**

Figure 4.4: Biodegradable polymer fiber from a PCL/CB combination. (A)Drawn polymer fiber; (B)The cross-section of a fiber.

Another biodegradable polymer with a low melting point of around 60°C but higher refractive index (1.52) - Polycaprolactone (PCL) used for microstructured optical fiber fabrication. PCL is degraded by hydrolysis in physiological condition and has received a great deal of attention as implantable biomaterial. In our design, PCL was used as a core material's while CB was used as cladding. The 2ocm preform was drawn into solid core fiber at temperatures of 176-178°C. Both core and cladding layers were well-drawn and produced solid core fiber as shown in Figure 4.4. The major problem of this fiber is poor transparency of PCL, leading to strong light attenuation.

4.3 Biodegradable microstructured optical fiber drawing

In Appendix article two "The prospective for the biodegradable microstructured optical fibers" (Dupuis et al., 2007) details of optical measurements of cellulose-based mPOFs. Loss of the microstructured polymer optical fiber discussed in section "Porous double-core polymer optical fiber" was measured by a standard cutback method. At $\lambda = 630nm$, the fiber transmission loss was between 1 and 2 dB/cm depending on a sample. Another experiment was also performed to find out changes in fiber transmission due to dissolution of a fiber microstructure.

Chapter 5

Conclusions and Discussions

5.1 Summary of accomplishments

In this thesis, we presented different configurations of microstructured polymer optical fibers and developed various techniques for fiber fabrications manufacture them. These novel mPOFs pave the way towards a novel of biocompatible and biodegradable optical fibers for applications in optical guiding, microfluidics and bio-medical sensing.

For Bragg fiebrs, the PMMA/PS and PVDF/PS material combiantion were chosen from many candidates because of their good optical, thermal chemical and mechanical compatibility. With these materials, we demonstrated that the solution evaporation coating technology could be applied to create make alternating layer structures on the inner surface of a cladding tube. The appropriate orthogonal solvents for each polymer were found. Acetone, cyclohexane, CH_2Cl_2 and methyl acetate solvent were used for PMMA, PS, PVDF and PC layer-by-layer deposition. Commercial PMMA and PC tubes were used as cladding material. The pretreatment of tubes including annealing and degassing is very important to make a high quality preform. We also optimized the coating parameters including rotation speed, nitrogen gas flow, drying temperature and drying time. Using these optimal parameters, we obtained up to 20 layer PMMA/PS and PVDF/PC fiber preforms.

We also developed the co-rolling method by using commercial and home-cast films

to make Bragg fiber preforms. The major advantage of this method is that it is easy to obtain a drawable multilayer structure, but it is hard to vary individual layer thicknesses.

The multilayer preforms made by the solution evaporation method suffered from bubbles during fiber drawing. For the preform made by the co-rolling method, high quality Bragg fibers were successfully fabricated. The drawing parameters, such as oven temperature, drawing speed, and feeding speed were studied for the optimization.

Finally, various biodegradable microstructured polymer optical fibers have been demonstrated for the first time. These fibers have great in bio-medical application. Optical fiber were fabricated successfully using cellulose's derivatives, PCL and PLA biocompatible polymer.

5.2 Future directions

Microstructured optical fiber technology has progressed rapidly over the last years. Polymers as material for MOF fabrication show many advantages over glass. The solution evaporation method that we developed has very attractive features like layer thickness control, and dopant treatment. Further experiments on solvent extraction from the resultant preforms are under way. Fabrication of mPOFs with fine features requires double step drawing, which we started to investigate.

Microstructured polymer optical fibers provide a platform for new classes of functional optical devices in data communication, biomedical and industrial fields. Further investigation into new composite materials and structures, such as combination of metals, polymer soft glass and nanoparticles, could allow fabrication of new fascinating photonics device.

REFERENCES

AEI: 2005, *(Automation Engineering Incorpotated) Process Manual*

Aldrich: 2005-2006a, *Catalog*

Aldrich: 2005-2006b, *Advancing Science Catalog*

Barton, G., Eijkelenborg, M., and Henry, G.: 2004, *Optical Fiber Technology* **10(4)**, 325

Birks, T., Knight, J., and Russell, P.: 1997, *Optics Letters* **22**, 961

Chen, W., Chang, Y., and Wei, M.: 2000, *Journal of Polymer Science Part B: Polymer Physics* **38(13)**, 1764

Co., M. R.: 1974, *U.K.Patent*, 1,431,157

Co., N. S.: 1976, *U.K.Patent*, 3,955,015

Cregan, R., Mangan, B., Knight, J., Birks, T., and Russell, P.: 1999, *Science* **285**, 1537

Dobrzynski, P., Kasperczyk, J., and Bero, M.: 1999, *Macromolecules* **32**, 4735

Dupuis, A., Guo, N., and Skorobogatiy, M.: 2007, *Optics Letters* **32**, 109

Ebendorff, H., Monro, T., and Eijkelenborg, M.: 2006, *Proc.OFC.Pap.* 7

Eijkelenborg, M., Large, M., Argyros, A., and Zagari, J.: 2001, *Optics Express* **9(7)**, 319

Fitt, A., Furusawa, K., and Monro, T.: 2001, *J. Lightwave Technol.* **19(12)**, 1924

Freudenrich, C.: January 2007, *http://electronics.howstuffworks.com/fiber-optic5.htm*

Guo, N., Gao, Y., Gauvreau, B., Rajabian, M., SkorobogataC., O., Pone, E., and Skorobogatiy, M.: 2006, *Journal of Materials Research* **21(9)**, 2242

Hasegawa, T.: 2004, *Optical Fiber and Method for Making Microstructured Optical*

Fibers, U.S.Patent, 6,766,088

Hidaka, T., Minamide, H., and Ito, H.: 2005, *JOURNAL OF LIGHTWAVE TECHNOLOGY* **23(8)**, 2469

Ishigure, T., Nihei, E., and Koike, Y.: 1996, *Applied Optics* **35**, 2048

Kaino, T., Jinguji, K., and Nara, S.: 1983, *Applied Physics Letters* **42**, 567

Kaiser, P. and Astle, H.: 1974, *The Bell System Technical Journal* **53**, 1021

Kapron, F., Keck, D., and Maurer, R.: 1970, *Applied Physics Letters* **17**, 423

Keiser, C.: 2000, *Optical Fiber Communcation*, McGraw-Hill

Knight, J., Birks, T., Cregan, R., and Russell, P.: 1998, *Electronics Letters* **34**, 1347

Knight, J., Birks, T., and Russell, P.: 1996, *Optics Letters* **21**, 1547

Koike, Y., Takezawa, Y., and Ohtsuka, Y.: 1989, *Applied Optics* **27**, 486

Nalwa, H.: 2004, *Polymer Optical Fibers*, American Scientific Publishers

Ohe, Y., Kadoma, Y., and Y.Imai: 1989, *Shika Zairyo Kikai (Japanese)* **8(4)**, 546

Ohtsuka, Y. and Hatanaka, Y.: 1976, *Applied Physics Letters* **29**, 735

Ohtsuka, Y. and Nakamoto, I.: 1976, *Appl.Phys.Lett* **29**, 559

Piskin, E.: 1995, *Journal of Biomaterials Science* **6**, 775

Pone, E., Dubois, C., Guo, N., Gao, Y., Dupuis, A., Boismenu, F., Lacroix, S., and Skorobogatiy, M.: 2006, *Optics Express* **14(13)**, 5838

Pratt, G.: 2005, *Journal of Materials Science* **10(5)**, 809

Ranka, J., Windeler, R., and Stentz, A.: 2000, *Optics Letters* **25**, 796

Richardson, D., Poletti, F., Leong, J., and Feng, X.: 2005, *Proceedings of 2005 IEEE/LEOS Workshop on Fibres and Optical Passive Components* pp 1–9

Tanya, M. and Ebendorff-Heidepriem, H.: 2006, *Annual Review of Materials Research* **36**, 467

Tayage, A., Kobayashim, T., and Nakatsuka, S.: 1997, *Japanese Journal of Applied Physics* **36**, 2705

Temelkuran, B., Hart, S., Benoit, G., Joannopoulos, J., and Fink, Y.: 2002, *Nature (London)* **420**, 650

Toyoda, N., Mishei, Y., and Murata, R.: 1995, *U.K.Patent*, 5,390,274

Wang, J., Li, M., and Nolan, D.: 2006, *Proc.OFC* 420

Wang, S.: 2003, *Method of fabricating Microstructured Optical Fibers*, U.S.Patent, 6,522,820

Webb, D., Kalli, K., Argyros, A., and Eijkelenborg, M.: 2005, *14th International Conference on Polymer Optical fiber* pp 19–21

Wu, S.: 1970, *J.Phys.Chem.* **74**, 632

Wypych, G.: 2001, *Handbook of Solvents, 1st ed.*, ChemTec Publishing

Yablonovitch, E.: 1987, *Physical Review Letters* **58**, 2059

Appendix A

Consecutive Solvent Evaporation and Co-Rolling Techniques for Polymer Multilayer Hollow Fiber Preform Fabrication

Consecutive solvent evaporation and co-rolling techniques for polymer multilayer hollow fiber preform fabrication

Yan Gao[a)]
Génie Physique, École Polytechnique de Montréal, Montréal H3C 3A7, Canada; and Génie Chimique, École Polytechnique de Montréal, Montréal H3C 3A7, Canada

Ning Guo[a)] and Bertrand Gauvreau
Génie Physique, École Polytechnique de Montréal, Montréal H3C 3A7, Canada

Mahmoud Rajabian
Génie Physique, École Polytechnique de Montréal, Montréal H3C 3A7, Canada; and Génie Chimique, École Polytechnique de Montréal, Montréal H3C 3A7, Canada

Olga Skorobogata
McGill University, Montréal, Montréal H3A 2T5, Canada

Elio Pone, Oleg Zabeida, and Ludvik Martinu
Génie Physique, École Polytechnique de Montréal, Montréal H3C 3A7, Canada

Charles Dubois
Génie Chimique, École Polytechnique de Montréal, Montréal H3C 3A7, Canada

Maksim Skorobogatiy[b)]
Génie Physique, École Polytechnique de Montréal, Montréal H3C 3A7, Canada

(Received 8 January 2006; accepted 20 April 2006)

All-polymer multilayer hollow core photonic fiber preforms were fabricated using consecutive deposition from a solvent phase of two polymers with high and low refractive indices (RI). Processing techniques for two polymer pairs—polystyrene (PS)/poly(methyl methylacrylate) (PMMA) and polycarbonate (PC)/poly(vinylene difloride) (PVDF)—were established. The fabrication process involved consecutive film deposition by solvent evaporation of polymer solutions on the inside of a rotating PMMA or PC tube, used as a cladding material. By injecting right volumes of the polymer solutions into a spinning tube the thickness of each layer could be reliably controlled from 20 to 100 μm. Proper selection of solvents and processing conditions was crucial for ensuring high optical and mechanical quality of a resultant preform, as well as compatibility of different polymer films during co-deposition. Preforms of 10 layers for PMMA/PS material combination and 15 layers for PVDF/PC were demonstrated. Fabrication of preforms with higher number of layers is readily possible and is only a question of preform fabrication time. An alternative method of preform fabrication by co-rolling of polymer bilayers is also presented in this paper, drawing of PMMA/PS, PVDF/PC fibers with up to 32 layers is demonstrated.

I. INTRODUCTION

High laser power delivery and sensing using near- and mid-infrared (IR) radiation (wavelength range 1–12 μm) have been active areas of applied optics in the past decade due to some crucial advantages offered by the IR wavelength range.[1–4] Hollow-core multilayer and microstructured fibers for radiation guiding in the IR[5–11] have recently received considerable attention as they promise important advantages over their solid-core counterparts in applications related to high power guidance at almost any IR wavelength for military, industry, and medical applications, as well as IR imaging and sensing. Recently, hollow-core fibers were also investigated for guidance of very long wavelengths ($\lambda \sim 100$ μm) in a THz range for chemical sensor and time-resolved measurement applications.[12,13] Because of its complexity, fabrication of such waveguides is an active field of research, in which any new manufacturing technology could enable a novel niche application. The main advantage of hollow-core photonic fibers over solid core fibers is in their ability to confine and guide radiation predominantly

[a)]These authors contributed equally to this work.
[b)]Address all correspondence to this author.
e-mail: maksim.skorobogatiy@polymtl.ca
DOI: 10.1557/JMR.2006.0271

inside a hollow core, thus dramatically reducing radiation propagation loss due to material absorption in the fiber materials, which is especially critical in the mid and far-IR ($\lambda > 3$ μm), where most of the materials are highly absorbing.

Four main methods have been identified for hollow-core fiber manufacturing. The first method is the deposition of metallo-dielectric films on the inside of a drawn capillary by liquid-phase coating[5,6]; technical difficulties in enforcing thickness uniformity in the resultant coatings limit fiber length ~10 m. The second method is a capillary stacking method[7–9] in which glass capillaries are arranged in a periodic manner and then drawn; so far such fibers have been demonstrated to only guide radiation with wavelengths smaller than 3 μm due to the non-transparency of silica material used in the fabrication. The third and relatively new method is deposition of uniform thin films on a pre-drawn substrate fiber by means of physical or chemical vapor deposition methods[10]; the main challenge of this technology is presumably uniformity of the resultant coatings and a low throughput due to a relatively slow deposition process. Finally, the fourth method uses a bilayer film rolling technique. Film rolling[11] starts with a deposition of a glass (chalcogenide) film on top of a polymer film; the resulting bilayer is then rolled around a mandrel tube, which is later etched away, and the final preform is drawn into a fiber. The main disadvantage of such a fiber is the questionable bio-compatibility of the material combination and challenges in fiber profile optimization due to a strictly periodic reflector geometry imposed by the fabrication method.

In this work, we consider an alternative to method of fabrication (described in Ref. 11) of hollow multilayer preforms. In the hollow multilayered waveguides, radiation confinement in a hollow core is achieved by reflection from a surrounding reflector consisting of a quasi-periodic sequence of thin layers of optically different materials with thicknesses comparable to a wavelength of the transmitted light. The total number of layers is typically 5–30. The critical step in realizing multilayer reflector is a selection of several optically different, but mechanically similar, materials that can be co-processed together to form a high optical quality multilayer preform. The preform, which is an enlarged (by a factor of 10 to 1000) copy of a fiber, is then placed into the furnace where it is heated above the polymer glass transition temperature and finally pulled into a fiber.

Fabrication of the all-polymer hollow multilayer fiber performs, which we describe in this paper, addresses a need for inexpensive and bio-friendly material combinations for use in biomedical applications. In our group, we have developed processing techniques and established several polymer material combinations to fabricate all-polymer hollow multilayer waveguide preforms by consecutive evaporation of polymer solutions on the inside of a rotating cladding tube. Ten to fifteen layer preforms based on polystyrene (PS)/poly(methyl methylacrylate) (PMMA) and polycarbonate (PC)/poly(vinylene difloride) (PVDF) material combinations have been fabricated. Among advantages of our fabrication method is precise control over the thickness and material composition of the individual layers, which enables fabrication of reflectors with highly optimized geometries. Moreover, functional materials can be incorporated into the layer structure by dissolving active elements such as laser dyes, nanoparticles, etc., in a polymer solution before coating. Potential biocompatibility of an all-polymer material combination opens the possibility of in vivo use of our fibers for laser delivery and sensing. The disadvantage of the proposed method is the necessity for a thorough solvent extraction from the deposited multiplayer, which limits the throughput of a fabrication process. The proposed methodology, combined with the co-rolling method described in Ref. 11 gives a very powerful all-polymer multilayer preform fabrication strategy where co-rolling could be used to create the "bulk" part of a photonic crystal reflector, while a moderate number of "custom-designed" functional layers can be deposited from a solvent phase.

This paper is organized as follows: we first describe materials and solvents used in the process. Then we describe processing conditions for different material combinations and challenges that arise during the co-deposition process. We then present polymer multilayer preforms of two different polymer combinations. Finally, we discuss co-rolling for polymer preform fabrication.

II. MATERIALS

In what follows, we describe fabrication of the fully polymeric multilayer hollow core fiber preforms based on either PS/PMMA or PC/PVDF pairs. Preforms were prepared by consecutive solvent evaporation of polymer solutions inside a rotating cladding polymer tube. Solvent evaporation of polymer solutions provides a versatile fabrication technique for deposition of polymer layers of variable thickness and composition.

Use of polymer pairs for fabrication of photonic waveguides imposes restrictions on materials, which have to be optically, chemically, and thermodynamically compatible. Optical applications require material transparency, thus making crystalline and semi-crystalline polymers less desirable for fiber drawing. Moreover, refractive indices in a polymer pair have to be appreciably different from each other (at least by 10%) to enable a sizable bandwidth for a periodic reflector.[14] Chemically, polymers have to be soluble in nontoxic organic solvents with low boiling points to enable efficient solvent extraction from the cast polymer films. Moreover, solvents

have to be "orthogonal" to each other so they do not cross-solve the two polymers during a bilayer deposition. Thermodynamically, polymers have to have similar processing temperatures to allow co-drawing.

We have found two polymer/solvent pairs to fulfill all the above requirements. These are the PS/PMMA and PC/PVDF material combinations. For many years, PMMA has been a material of choice for plastic optical fiber fabrication, while PS and PC have been investigated as materials for fiber protective coatings.[15] PS and PMMA blends and co-polymers have been considered in many publications for self-assembly of nanostructures,[16–20] as well as multilayer thin film formation.[21–26] PVDF is a semicrystalline polymer of low refractive index (RI) with partially fluorinated chain structure and is a relatively unexplored polymer for optical applications. Prior work on PVDF and PC blends as well as multilayer thin films is presented in Refs. 27 and 28. Compared with most fluorinated polymers, especially perfluorinated polymers, PVDF is quite inexpensive and shows good solubility in organic solvents. In the present study, a PVDF copolymer containing hexafluoropropylene was chosen because it has lower crystallinity and a lower melting point than a homopolymer; consequently, it also has better solubility than a homopolymer. Glass transition temperatures of the PS/PMMA and PC/PVDF polymer pairs are well matched with differences of only 5 and 14 °C, respectively. Refractive index mismatches between the constituents of each pair are respectively Δn = 0.12 and Δn = 0.18 over the visible and IR spectra. In the Appendix, we present in greater detail some of the optical properties of the studied polymer films in the visible and IR regions. Material parameters of each polymer pair are summarized in Table I, showing good matching of polymer physical and thermodynamic properties.

PS, PMMA, and PC in granules were purchased from Aldrich. PVDF (Solef21216) in powder form was provided by Solvay Solexis. PC and PMMA tubes were purchased form McMaster Carr Canada and cut into 12-in.-long pieces.

Prior to usage, both PMMA and PC tubes were cleaned with a water solution of a generic commercial surfactant. PMMA tubes were further washed in an ultrasonic bath. After further cleaning with 95% ethanol, PMMA and PC tubes were annealed and degassed in vacuum oven overnight at 70 and 120 °C, respectively.

TABLE I. Physical parameters of polymer materials: T_p = thermal processing temperature; T_g = glass transition temperature; T_m = melting temperature; RI = refractive index.

Polymer	RI at 1050 nm	RI difference at 1050 nm	T_g (°C)	T_m (°C)	Difference in T_p (°C)	Density (g/cm^3)
PS	1.60	0.12	100		5	1.05
PMMA	1.48		105			1.19
PC	1.58	0.18	149		14	1.20
PVDF	1.40		−30	135		1.78

III. SOLVENTS

For a given polymer pair, the first step is to choose low boiling point, non-toxic solvents. The orthogonal characteristics of selected solvents must be ensured with respect to cross-solving of the polymers in a pair. Thus, to make sure that during the next layer coating the previously coated layer is not destroyed, a solvent to the second component of a polymer pair must be a non-solvent to the first one and vice versa. In addition, other properties of solvents such as vaporization velocity, boiling point, relative toxicity, and price must be considered. Normally, more volatile organic solvents with low boiling points are preferred because it is easier to extract them after the deposition process. Using solubility parameters of polymers and solvents for guidance,[29] for each polymer pair several solvent pairs were tested and compared. Solvents used in this study are listed in Table II, where (+) signifies solubility and (−) signifies non-solubility of a polymer in a given solvent; (%) reflects optimal polymer concentrations in a given solvent.

Although PVDF copolymer-containing hexafluoropropylene shows good solubility compared to most fluorinated polymers, the choice of organic solvents remains quite limited. Commonly used solvents for casting PVDF films such as *N,N*-dimethylacetamide, *N,N*-dimethylformamide, 1-methylpyrrolidone, and dimethyl sulfoxide are not suitable as they all dissolve PC to some extent. We found that such solvents as acetone, 1-butanone, acetonitrile, and methyl acetate dissolve PVDF copolymer but not the PC. Because 1-butanone and acetonitrile formed only metastable PVDF solutions, we concentrated our attention on acetone and methyl acetate as PVDF solvents.

In our work, we have also used solvent blends to increase adhesion between the immiscible polymer pairs. Thus, a small percentage of a common solvent could be added to the otherwise orthogonal solvent pair to promote stronger adhesion through interface fusion between the two polymers.

All solvents (obtained from Aldrich) were reagent grade and were used as received. Polymers were dissolved in selected solvents in a covered flask with a magnetic stirrer at room temperature or elevated temperatures to prepare solutions of 5–10% concentration. PMMA and PS solutions were then ultrasonically degassed for about 1 h in a water bath.

IV. MULTILAYER FILM DEPOSITION PROCESS

Depending upon desired thickness of a polymer layer (in a range of 20–100 μm) a corresponding amount of polymer solution is injected into the polymer tube. The

TABLE II. Orthogonal solvents for the two different polymer pairs: (+) is soluble, (−) is not soluble. In parentheses, we indicate optimal polymer concentration in a solvent.

	Solvents							
Polymer	Cyclohexane/ toluene (95/5)	CH_3CN	CCl_4	Cyclohexane/ CCl_4 (95/5)	CH_3COCH_3	$CHCl_3$ or CH_2Cl_2	CH_3COOCH_3	Cyclohexanone
PS	+(5%)	−	+(5%)	+(5%)	−			
PMMA	−	+(5%)	−	−	+(5%)			
PC					−	+(5–10%)	−	+
PVDF					+(5%)	−	+(5%)	+

tube is then placed horizontally into a rotational stage with one end connected to a nitrogen inlet and another end connected to a fume exhaust. The tube is then rotated with a speed of 1000-2000 rpm. When solvent is evaporated (by visual inspection), the tube is put into an oven to completely remove the residual solvent. A temperature schedule is used with several hours of evaporation at 30–50 °C followed by several hours at 50–70 °C and slow cooling. For a selected solvent pair, coating conditions such as nitrogen flow velocity, rotating velocity of tube, and solution concentration, must be optimized to increase quality of the deposited films. Spin coating is performed under a constant nitrogen flow to prevent moisture and dust in the air from being embedded in a coated film. However, large nitrogen flow rates would cause ripples or bubbles that can be incorporated in the film. We found optimal flow rates to be 0.1–0.5 ml/min at the beginning of the process and 1–3 ml/min at the end of the deposition process when most of the solvent has already evaporated. Polymer solution concentrations of 5–10% were tested with optimal concentrations listed in Table II. Rotation speeds of a spin coater between 1000 and 2000 rpm were found to produce the smoothest preforms.

V. PS/PMMA POLYMER COMBINATION

A. CCl_4/acetonitrile(CH_3CN) solvent pair

For the PS/PMMA pair, CCl_4/acetonitrile (CH_3CN) was initially used for coating. PS solution in CCl_4 gave a perfectly smooth first layer on a PMMA tube. PMMA solution in acetonitrile also gave a good second layer, which was optically transparent and well attached to the first layer. However, a second coated PS layer would exhibit wrinkles at the end of a tube connected to the nitrogen purge no matter how small the nitrogen flow was. When coating the third PS layer from CCl_4 solution, the previously coated layers would crack. In general, backbones of the PS chains tend to stretch in a good solvent such as CCl_4, causing accumulation of residual stress during the relatively fast evaporation process. Cracking could also be caused by CCl_4 diffusion into the previously coated PS layers where it attacks the points of high residual stress. Preforms with up to 2 PS layers were fabricated with CCl_4/acetonitrile solvents.

B. [Cyclohexane (C_6H_6) + 5% toluene (C_7H_8)]/acetonitrile (CH_3CN) solvent pair

Cyclohexane has a solubility parameter similar to that of CCl_4. However, when PS was dissolved in cyclohexane at elevated temperatures, the polymer solution became inhomogeneous when cooled during storage. Toluene is a good solvent for both PS and PMMA. When 5% toluene was added into cyclohexane, it dissolved PS very well, even at room temperature. Thus, the (cyclohexane + 5% toluene)/acetonitrile combination was tested for the PS/PMMA pair coating. Unlike CCl_4, a mixture of cyclohexane and toluene is not as strong of a solvent as CCl_4. PS film cast from a (cyclohexane + 5% toluene) solution gave a mainly transparent and smooth first PS layer. Casting PMMA layer from acetonitrile solution resulted in a clear and well-attached second layer. The third layer from a PS solution in (cyclohexane + 5% toluene) also gave a mainly transparent and smooth PS film well attached to the second PMMA layer. However, starting from the third layer, micro-bubble formation was observed. Using this layer-by-layer process, a PMMA tube was coated with up to 6 alternative PS and PMMA films. The resulting preform consisted of a 3.5-mm-thick PMMA tube with an inner diameter of 25 mm and 6 alternative PS and PMMA layers with thicknesses of 80 and 50 μm, respectively.

C. [Cyclohexane (C_6H_6) + 5%CCl_4]/ [acetonitrile(CH_3CN) or acetone(C_3H_6O)] solvent pairs

Using CCl_4 instead of toluene in a solvent blend leads to a considerable improvement in the layer-by-layer deposition process. Coating quality was improved further when acetonitrile was substituted by acetone to dissolve PMMA. When coating was made at elevated temperatures (30–60 °C), considerable improvements in layer morphology and transparency were achieved; preforms of up to 12 alternative layers were readily obtained with both (cyclohexane + 5% CCl_4)/acetone and a (cyclohexane + 5% CCl_4)/acetonitrile solvent pairs for PMMA and

PS, respectively. In Fig. 1, a ten-layer preform and its cross section are shown. Here and in the following figures, optical micrographs were obtained on thin samples under reflected light and the non-polarizing mode of a Leitz microscope; the samples were cut from the tube with a diamond saw. In Fig. 1(b), layers corresponding to different polymers are clearly distinguishable due to different reflective properties of polymer films featuring non-identical refractive indices.

The preform in Fig. 1(a) is transparent with a smooth inner surface and without ripples; only a few bubbles at the end of the tube were observable. When the same coating was repeated at room temperature, bubbles and ripples appeared in the multilayer structure. Elevated temperature coating is superior to room temperature coating in two ways. First, at elevated temperatures, cyclohexane dissolves PS better than at room temperatures, increasing chain mobility and preventing polymer chain segments from crystallization. Second, elevated temperatures accelerate solvent evaporation and solvent removal from the polymer matrix. Furthermore, we observed that a multilayer created with (cyclohexane + 5% CCl_4)/acetone solvent pair exhibits sharper interfaces than a multilayer created with (cyclohexane + 5% CCl_4)/acetonitrile solvent pair. Difference in the interfacial structures could be attributed to different degrees of swelling of a PS layer by acetone and acetonitrile solvents causing various penetration depths of PMMA molecular chains into PS polymer layers. Multilayer preforms fabricated under these conditions, with the last layer exposed to the air being PMMA, stay transparent for many months with only a faint onset of opaqueness. After several months of storage, a number of microcracks appeared inside the multiplayer, suggesting relaxation dynamics of a stressed multilayer.

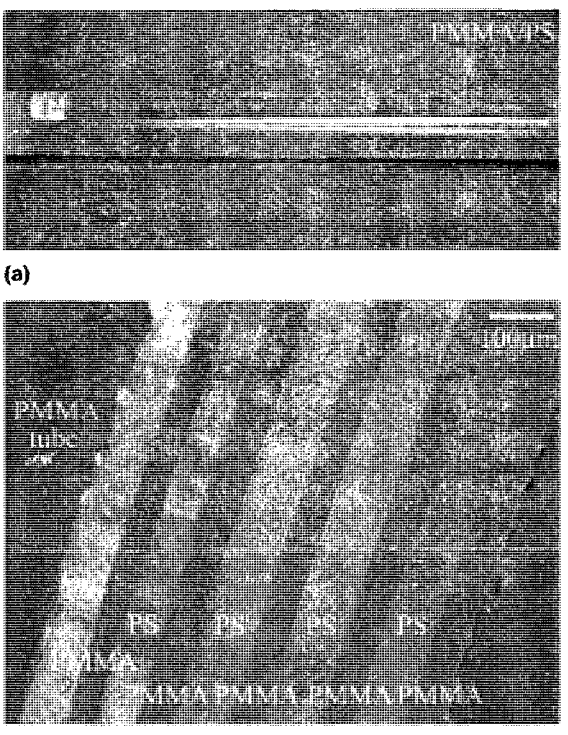

FIG. 1. (a) Ten-layer PMMA/PS preform using (cyclohexane + 5% CCl_4)/acetonitrile solvents. (b) Optical micrograph of a preform cross-section.

D. Degradation of optical properties of solvent-cast PS films during storage

An important question related to the quality of solvent cast films is about degradation of film optical properties during storage due to trapped solvents (solvent-induced crystallization) and interaction with the environment. While in all our experiments PMMA films were always transparent, we observed that opaqueness of PS films depended strongly on a solvent extraction method used in film casting, as well as on PS film exposure to the elements during storage. Thus, PS films exposed to air would typically become opaque in a matter of several days. However, when PS film was stored in vacuum it would stay transparent for several months. When PS film was protected on both sides by the PMMA polymer layers, it would remain transparent even after a year of storage when prepared from (cyclohexane + 5% CCl_4)/acetone at elevated temperatures (due to efficient solvent extraction). However, a PS film protected by the two PPMA layers would become opaque in a matter of days if multilayer was prepared with (cyclohexane + 5% toluene)/acetonitrile at room temperature (due to non-efficient solvent extraction).

Scanning electron microscopy (SEM) was performed on the surfaces of various PS films to understand the above phenomenon. Because the PS layer was well attached to the PMMA tube after coating (due to partial penetration of PS into a swelled PMMA matrix), it was difficult to separate it for SEM observations without destroying the film surface. Instead, we cast PS film on the inside of a quartz tube using solvents and processing conditions identical to the ones described in the previous subsections. After the deposition, it was easy to detach an initially transparent PS film from the quartz substrate. In a typical experiment, the PS films were either left exposed to air or stored in vacuum. PS film stored in the air, after several days, became somewhat opaque with many white dots peppered in the film. After one week of storage, individual white dots coalesced into an opaque film with SEM revealing a fully developed crystalline phase [Fig. 2(a)]. For comparison, SEM performed on the surface of a PS film stored in vacuum, showed the absence of crystallization even after several months of storage [Fig. 2(b)]. Although it seems that the amount of trapped solvent and exposure to the elements are the main factors

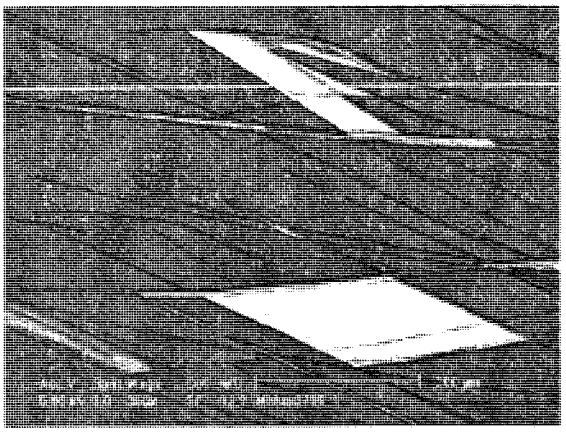

(a)

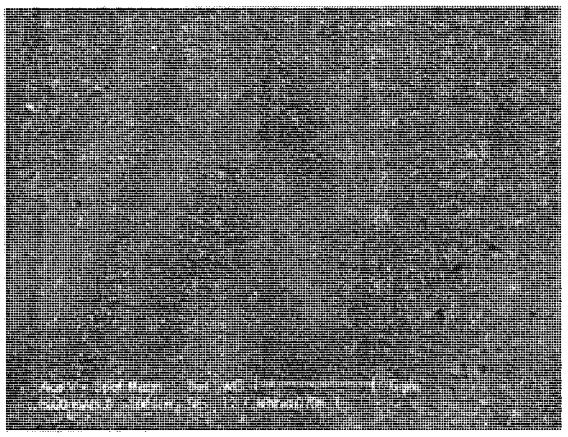

(b)

FIG. 2. SEM images of PS films deposited from various solvents onto a glass tube: (a) film cast from (cyclohexane + 5% toluene) at room temperature, stored in air, crystalline phase apparent after one week of storage and (b) film cast from a (cyclohexane + 5% CCl_4) solution at 45 °C, stored in vacuum. Unlike the film shown in (a), no crystallization is observed even after several months of storage.

influencing the long-term optical stability of PS films, more quantitative study is still needed.

E. PC/PVDF combination

For a PC/PVDF pair with a PC tube as a cladding material, several new problems appeared during coating: cracking of the PC tube, appearance of milky color in both the PC tube and deposited PC layers, and detachment of the coated layers. Thus, a non-annealed PC tube would fracture immediately when exposed to acetone, which was originally used as a solvent for PVDF. In general, it was observed that PC exhibits relatively low resistance to organic solvents.[30] This is in part due to the relatively high free volume of loosely packed rigid PC chains, which allows efficient solvent penetration into the polymer matrix. In non-annealed tubes, the penetrated solvent attacks points of high stress and leads to the appearance of a maze of micro-cracks, each several millimeters in length. PC tubes annealed at 120 °C for several days in a vacuum oven demonstrated considerably improved resistance to solvents. Although micro-cracks were no longer observed in annealed PC tubes when exposed to PVDF solution in acetone, occasionally, a single macro-crack of several centimeters of length would appear. Finally, we have found that when PVDF solution in methyl acetate was used instead of acetone, the probability of crack appearance in PC tubes was greatly reduced. No matter what solvent was used to dissolve PVDF, the milky color of the PC tube always appeared when PVDF layers were deposited.

F. (Acetone or methyl acetate)/(CH_2Cl_2 or $CHCl_3$) solvent pair

The first deposited PVDF layer from either acetone or methyl acetate was always shiny, smooth, and well attached to the PC tube. The second PC layer cast from either CH_2Cl_2 or $CHCl_3$ coated on the top of the first PVDF layer was also shiny, smooth, and well attached to the previous layer. When a third layer of PVDF was coated, although it was still smooth, the three combined layers would frequently detach from the PC tube, and each layer could be readily separated by peeling. The low adhesion strength between PC and PVDF is a result of their semi-compatibility due to high interfacial tension between C–H-based PC and C–F-based PVDF.[28]

G. (Acetone or methyl acetate + cyclohexanone)/(CH_2Cl_2 or $CHCl_3$) solvent pair

To improve adhesion strength between the adjacent layers, cyclohexanone was added to a PVDF solution in acetone or methyl acetate. Cyclohexanone dissolves PC very well; however, only a metastable PVDF (Solef21216) solution formed in a pure cyclohexanone. Improved interlayer adhesion was achieved due to solvent wetting of both the PC and PVDF layers, thus causing interpenetration of the polymer chains in the adjacent layers. Two PVDF/PC based preforms were initially fabricated. The first preform contained 7 layers; a mixture of acetone and cyclohexanone (volume ratio of 75 to 25) was used to dissolve PVDF while CH_2Cl_2 was used to dissolve PC. The second preform contained 5 layers; a mixture of methyl acetate and cyclohexanone (volume ratio of 95 to 5) was used to dissolve PVDF, and CH_2Cl_2 was used to dissolve PC. The addition of cyclohexanone into PVDF solution in acetone or methyl acetate considerably improved adhesion between the PVDF and PC layers. Unlike in the case of a PVDF film cast from pure acetone or methyl acetate solvent (for which a complete layer detachment was observed), only a small detachment at the ends of a tube was observed when solvent blends were used, starting with the fifth layer for

acetate + cyclohexanone and the seventh layer for methyl acetate + cyclohexanone. Moreover, addition of cyclohexanone considerably suppressed the occurrence of large cracks in the PC tube. It was further established that high cyclohexanone content in a PVDF solution caused degradation in the smoothness of the coated polymer films, such as appearance of wrinkles. Thus, for example, 5–10% cyclohexanone content in a methyl acetate solution produced smoother layers and sharper interfaces than 25% cyclohexanone content.

H. (Acetone or methyl acetate + $CHCl_3$)/(CH_2Cl_2 or $CHCl_3$) solvent pair

Addition of cyclohexanone into acetone or methyl acetate improved adhesion between PC and PVDF layers; however, because cyclohexanone has a high boiling point (156 °C), removing residual solvent at elevated temperatures (>50 °C) and in vacuum after each PVDF layer coating proved to be time consuming, thus making the use of cyclohexanone unfavorable. Low boiling point $CHCl_3$ was then used instead of cyclohexanone to wet the interfaces, but $CHCl_3$ and CH_2Cl_2 solvents were still used to dissolve PC. For PVDF solutions, 10–20% $CHCl_3$ was added into a PVDF solution in methyl acetate under strong stirring to avoid precipitation of PVDF until the solution became homogeneous. A multilayer of 15 layers with 40 μm (PVDF) and 20 μm (PC) layer thickness was then coated on the inside of the PC tube (Fig. 3), showing good adhesion between layers. Small detachment of the multilayer from the tube was observed near the tube edge after coating five layers; however no detachment was observed in the rest of the tube.

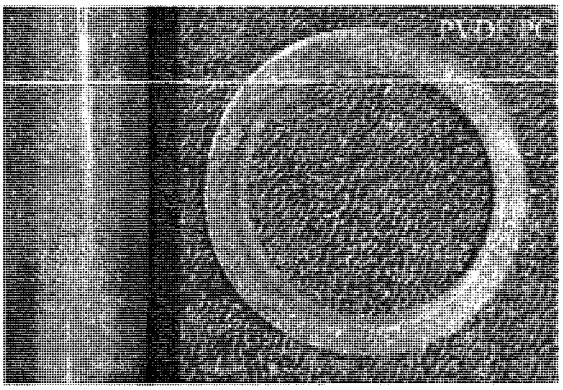

(a)

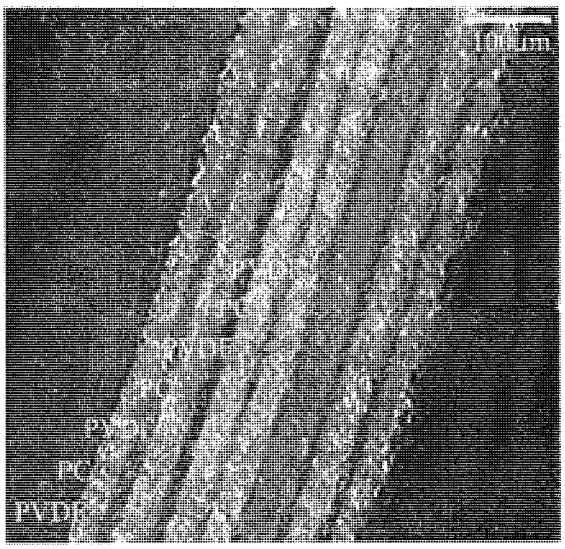

(b)

FIG. 3. (a) Fifteen-layer PVDF/PC preform. (b) Optical micrograph of the preform cross section.

I. Preform fabrication by co-rolling of polymer films

We briefly mention an alternative method of all-polymer multilayer preform fabrication by co-rolling of several different polymer films around the same mandrel. The main advantage of this method is in the absence of the multiple solvent evaporation steps, while the main disadvantage is in the fact that it is difficult to vary the thicknesses and compositions of individual layers. Using this method, we demonstrated 32 layer preforms of PS/PMMA, PC/PVDF, and PS/PVDF material combinations. We used both commercial and home-cast films. Commercial films were provided by the following companies: PVDF, Kynar Flex 2800 by CS Hyde Company; PC, Europlex 99506; PMMA, Europlex 99710 by Degussa, Advanced Polymer Shapes Rohm Gmbh & Co.; and PS, The Dow Chemical Company. Home-cast bilayer films were prepared by polymer solution evaporation on a 12 × 8 in. glass or metal surface, followed by consecutive casting of another polymer on the top of a first one using the orthogonal solvent technique introduced in this paper. The choice of solvents and processing conditions for bilayer formation was similar to the ones described previously in this paper. The resulting bilayer films with thickness of 50–100 μm were then rolled onto a Teflon mandrel with a consecutive consolidation of a rolled preform at temperatures above the typical thermal transition temperature of a polymer pair. Resulting preforms were then successfully drawn into fibers. In Fig. 4, we show drawn fibers with a 1:20 draw-down ratio of their outside diameter to that of a preform for PVDF/PC and PMMA/PS material combinations.

VI. CONCLUSIONS

In this paper, we have described a novel methodology for fabrication of hollow all-polymer photonic crystal fiber preforms. In particular, we have developed a methodology for the deposition of PS/PMMA and PC/PVDF

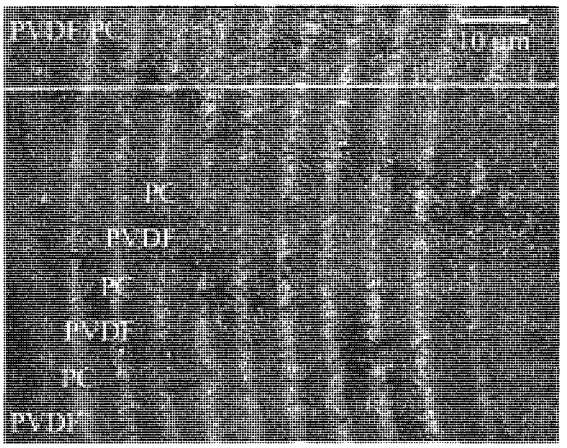

(a)

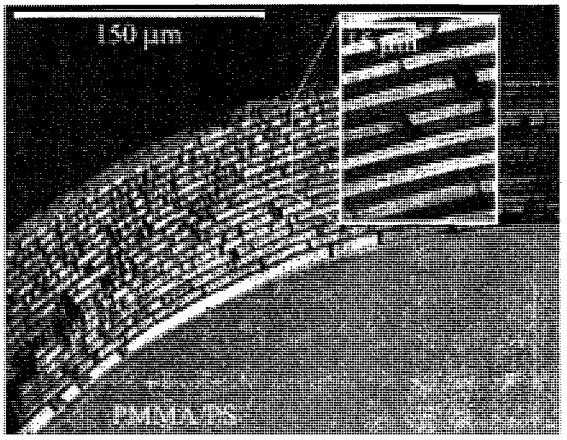

(b)

FIG. 4. (a) Cross section of a drawn 21-layer PVDF/PC fiber. (b) Cross section of a drawn 32-layer PMMA/PS fiber.

polymer multilayers (more than 10 layers with individual layer thicknesses of 25–100 μm) by consecutive evaporation from a solvent phase onto the inside of a rotating polymer cladding tube. The advantage of this layer-by-layer method is in the freedom that it offers in adjusting thicknesses of the individual layers, as well in the possibility of incorporation of functional elements such as laser dyes, quantum dots, etc., into a chosen layer to ultimately implement enhanced optical functionalities of the resultant fiber. The disadvantage of this method is in the requirement of a thorough solvent extraction from a resulting multilayer, which limits the throughput of a process.

We believe that the industrial strength process for fabrication of low-cost, yet functional, multilayer all-polymer photonic crystal fibers will involve both the co-rolling technique to create the "bulk" of the photonic crystal reflector and subsequent deposition (from a solvent phase) of a moderate number of specialty "functional" layers.

REFERENCES

1. T. Katsuyama and H. Matsumura: *Infrared Optical Fibers* (Adam Hilger, Bristol, UK, 1989), pp. 1, 231.
2. M. Saito and K. Kikuchi: Infrared optical fiber sensors. *Opt. Rev.* **4,** 527 (1997).
3. J. Sanghera and I. Aggarwal: *Infrared Fiber Optics* (CRC, Boca Raton, FL, 1998), pp. 1, 368.
4. *Optical Sensors and Microsystems: New Concepts, Materials, Technologies,* 1st ed., edited by S. Martellucci, A.N. Chester, and A.G. Mignani (Springer, New York, 2000), pp. 1–326.
5. J.A. Harrington: A review of IR transmitting, hollow waveguides. *Fiber Integr. Opt.* **19,** 211 (2000).
6. Y.W. Shi, K. Ito, Y. Matsuura, and M. Miyagi: Multiwavelength laser light transmission of hollow optical fiber from the visible to the mid-infrared. *Opt. Lett.* **30,** 2867 (2005).
7. P. Russell: Photonic crystal fibers. *Science* **299,** 358 (2003).
8. C.M. Smith, N. Venkataraman, M.T. Gallagher, D. Muller, J.A. West, N.F. Borrelli, D.C. Allan, and K.W. Koch: Low-loss hollow-core silica/air photonic bandgap fibre. *Nature* **424,** 657 (2003).
9. M.A. van Eijkelenborg, A. Argyros, G. Barton, I.M. Bassett, M. Fellew, G. Henry, N.A. Issa, M.C.J. Large, S. Manos, W. Padden, L. Poladian, and J. Zagari: Recent progress in microstructured polymer optical fibre fabrication and characterisation. *Opt. Fiber Technol.* **9,** 199 (2003).
10. T. Katagiri, Y. Matsuura, and M. Miyagi: Photonic bandgap fiber with a silica core and multilayer dielectric cladding. *Opt. Lett.* **29,** 557 (2004).
11. B. Temelkuran, S.D. Hart, G. Benoit, J.D. Joannopoulos, and Y. Fink: Wavelength-scalable hollow optical fibres with large photonic bandgaps for CO2 laser transmission. *Nature* **420,** 650 (2002).
12. T. Hidaka, H. Minamide, H. Ito, J. Nishizawa, K. Tamura, and S. Ichikawa: Ferroelectric PVDF cladding terahertz waveguide. *J. Lightwave Technol.* **23,** 2469 (2005).
13. J. Harrington, R. George, P. Pedersen, and E. Mueller: Hollow polycarbonate waveguides with inner Cu coatings for delivery of terahertz radiation. *Opt. Express* **12,** 21 (2004).
14. M. Skorobogatiy: Efficient anti-guiding of TE and TM polarizations in low index core waveguides without the need of omnidirectional reflector. *Opt. Lett.* **30,** 2991 (2005).
15. A. Weinert: *Plastic Fiber Optics: Principles, Components, Installation* (Wiley-VCH, Berlin, Germany, 1999), pp. 1–154.
16. Y.M. Gong, Z.J. Hu, Y.Z. Chen, H.Y. Huang, and T.B. He: Ring-shaped morphology in solution-cast polystyrene poly(methyl methacrylate) block copolymer thin films. *Langmuir* **21,** 11870 (2005).
17. Y. Xuan, J. Peng, L. Cui, H.F. Wang, B.Y. Li, and Y.C. Han: Morphology development of ultrathin symmetric diblock copolymer film via solvent vapor treatment. *Macromolecules* **37,** 7301 (2004).
18. K.W. Guarini, C.T. Black, and S.H.I. Yeuing: Optimization of diblock copolymer thin film self assembly. *Adv. Mater.* **14,** 1290 (2002).
19. S. Walheim, M. Boltau, J. Mlynek, G. Krausch, and U. Steiner: Structure formation via polymer demixing in spin-cast films. *Macromolecules* **30,** 4995 (1997).
20. K. Tanaka, A. Takahara, and T. Kajiyama: Film-thickness dependence of the surface structure of immiscible polystyrene/poly(methyl methacrylate) blends. *Macromolecules* **29,** 3232 (1996).
21. S.Y. Heriot and R.A.L. Jones: An interfacial instability in a transient wetting layer leads to lateral phase separation in thin spin-cast polymer-blend films. *Nat. Mater.* **4,** 782 (2005).
22. T. Podgrabinski, E. Hrabovska, V. Svorcik, and V. Hnatowicz:

Characterization of polystyrene and doped polymethylmethacrylate thin layers. *J. Mater. Sci. Mater. Electron.* **16,** 761 (2005).
23. M. Kim, R. Nagarajan, J.H. Snook, L.A. Samuelson, and J. Kumar: Nanostructured assembly of homopolymers for a flexible Bragg grating. *Adv. Mater.* **17,** 631 (2005).
24. E.M. Ivan'kova, M. Krumova, G.H. Michler, and P.P. Koets: Morphology and toughness of coextruded PS/PMMA multilayers. *Colloid Polym. Sci.* **282,** 203 (2004).
25. M. Harris, G. Appel, and H. Ade: Surface morphology of annealed polystyrene and poly(methyl methacrylate) thin film blends and bilayers. *Macromolecules* **36,** 3307 (2003).
26. C.H. Lin and A.C.M. Yang: Stability of the superplastic behavior of glassy polystyrene thin films in sandwich structures. *Macromolecules* **34,** 4865 (2001).
27. J. Feng, L. Weng, L. Li, and C. Chan: Compatibilization of polycarbonate and poly(vinylidene fluoride) blends studied by time-of-flight secondary ion mass spectrometry and scanning electron microscopy. *Surf. Interface Anal.* **29,** 168 (2000).
28. N. Moussaif, P. Marechal, and R. Jerome: Ability of PMMA to improve the PC/PVDF interfacial adhesion. *Macromolecules* **30,** 658 (1997).
29. *Handbook of Solvents,* 1st ed., edited by G. Wypych (ChemTec Publishing, Toronto, Canada, 2001), pp. 1–1680.
30. A. Pirori and L. Nicolais: The kinetics of surface craze growth in polycarbonate exposed to normal hydrocarbons. *J. Mater. Sci.* **18,** 1466 (1983).
31. A. Harlin, H. Myllymäki, and K. Grahn: Polymeric optical fibres and future prospects in textile integration. *AUTEX Res. J.* **2,** 1 (2002).

APPENDIX: OPTICAL PROPERTIES OF THE POLYMER FILMS

Optical properties of the polymer films in the visible and IR regions were studied experimentally using spectroscopic ellipsometry and Fourier transform infrared (FTIR) measurements. Four planar polymer films were cast from solvents in a glass Petri dish using the processing conditions described in this paper. Round samples of 5 cm in diameter were prepared with the following thicknesses measured using a Mitutoyo digital micrometer: PMMA, 34 ± 4 μm; PS, 21 ± 3 μm; PVDF, 18 ± 4 μm; PC, 83 ± 4 μm.

The refractive index n of the polymers was determined by variable angle spectroscopic ellipsometry (VASE) in the visible and near-infrared regions between 300 and 1700 nm using angles of incidence from 45° to 65° with a step of 5°. The data were fitted with the Cauchy dispersion model and Urbach absorption tale using the WVASE32 software (J.A. Woollam Co.; curves in Fig. 5). For two values of the wavelength, namely 550 and 1050 nm, additional VASE measurements were performed using angles of incidence from 35° to 75° with a step of 1°. These data were fitted using the same model independently from the spectroscopic data (special symbols in Fig. A1).

Optical transmittance of the above-mentioned films was then measured with a spectrophotometer (Lambda 19, Perkin Elmer) and with FTIR spectrometer

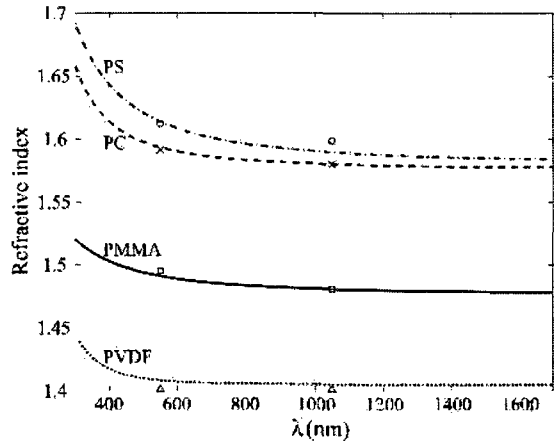

FIG. A1. Refractive index of the PMMA, PS, PVDF, and PC polymer films in the visible and near infrared regions.

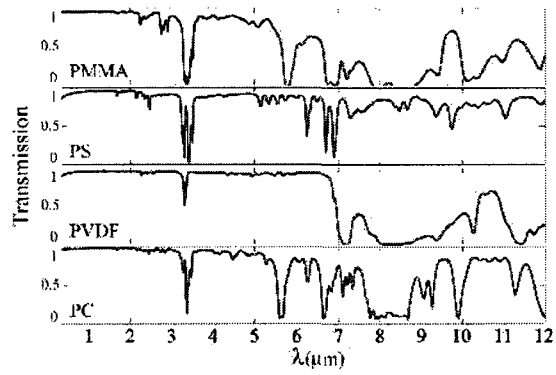

FIG. A2. Normalized transmission spectra through the 20-μm-thick PMMA, PS, PC, and PVDF polymer films in the infrared region.

(IR-VASE, J.A. Woollam Co.) in the range of 200–3200 nm and 2.50–25.0 μm, respectively. To simplify comparison of transmission properties of films of various thicknesses, the transmission spectra in Fig. A2 are normalized to a thickness of 20 μm. As our film samples were not smooth enough, uncertainty due to additional scattering losses did not allow us to reliably extract bulk absorption losses of the materials. However, transmission spectra still provide a good indication of the material transparency regions in the infrared. For more details on bulk absorption losses of PMMA, PS, and PC polymer materials in the visible, refer to Ref. 31. From Fig. 6, it follows that all four materials are relatively transparent in the visible and near infrared. Another transparency window for all four materials is around 3 μm, where Er:yttrium aluminum garnet (YAG) lasers are readily available, followed by a region between 3.5 and 5.5 μm. Finally, PVDF/PC or PVDF/PS combinations exhibit transparency windows around 10.6 μm, corresponding to a CO_2 laser emission line.

Appendix B

The prospective for the biodegradable microstructured optical fibers

Prospective for biodegradable microstructured optical fibers

Alexandre Dupuis, Ning Guo, Yan Gao, Nicolas Godbout, Suzanne Lacroix, Charles Dubois, and Maksim Skorobogatiy

École Polytechnique de Montréal, Génie Physique, C.P. 6079, succursale Centre-Ville Montreal, Québec H3C3A7, Canada

Received July 27, 2006; revised October 15, 2006; accepted October 20, 2006; posted October 20, 2006 (Doc. ID 73530); published December 23, 2006

We report fabrication of a novel microstructured optical fiber made of biodegradable and water soluble materials that features ~1 dB/cm transmission loss. Two cellulose butyrate tubes separated with hydroxypropyl cellulose powder were codrawn into a porous double-core fiber offering integration of optical, microfluidic, and potentially drug release functionalities. © 2006 Optical Society of America

OCIS codes: 060.2280, 170.3890.

As fabrication of microstructured optical fibers (MOFs) matures, there is a growing trend of integrating multiple functionalities into the same fiber. In particular, microstructured polymer optical fibers have recently received much attention, as several preform fabrication techniques have been established that use a variety of moderately priced polymer materials. Thanks to the biofriendly polymer material composition, many microstructured polymer optical fibers having porous structure have been designed with a view to biomedical applications. Furthermore, proper design of the fiber structure can allow other functionalities, such as fluorescence detection enhancement, laser power delivery, and controlled release of pharmaceuticals.

Sensing by using MOFs[1–5] relies on detecting changes in fiber transmission properties when fiber pores are filled with analyte. A number of porous fibers have been developed, featuring judiciously arranged holes,[6–8] randomly placed holes,[9–11] Fresnel fibers,[11] and hollow multilayer fibers.[12–15] Several all-polymer-based hollow photonic bandgap fibers were also recently demonstrated,[8,16] potentially offering operation with gas- or liquid-filled cores. Liquid-filled fibers in a classical hexagonal arrangement for sensing and microfluidics were considered in Refs. 2 and 17–19.

Regardless of the geometry, a crucial step in making MOF biosensors is sensitizing the inner surface of the fiber pores (holes) with a bioactive material to allow selective binding and consequent detection of a biological analyte. Jensen *et al.*[20] and Rindorf *et al.*[21] demonstrated fluorescence detection of selectively captured antibodies and DNA labeled with fluorescent markers. They also found that deposition of a sensing biolayer onto a polymer surface is easier than onto a glass one, thus making polymer fibers better suited for biosensing than glass.

Functionalities of MOFs can be further enhanced by adding a second core. Traditionally, double-cladding/core MOFs were used for directional coupling[22] and dispersion management. Recently such fibers have been also used to enhance the sensitivity of fluorescence microscopy[23,24] by permitting single-mode delivery of the excitation pulse through a smaller core and efficient collection of the signal (fluorescent light) by the larger multimode outer core. Beyond sensing, hollow-core MOFs[12–15] have been demonstrated to deliver tens of watts of laser power almost anywhere in the IR, providing flexible power delivery from the medically important Nd:YAG, Er:YAG, and CO_2 lasers.

An intriguing possibility is to incorporate optical, sensing, and medical treatment functionalities into the same biocompatible fiber to create a highly integrated and self-sufficient medical system. In one possible scheme, the tissue is first exposed to high-power laser light transmitted through the fiber core, and then integrated optical sensors evaluate the results of tissue treatment, while the porous microfluidic structure impregnated with water-soluble pharmaceuticals allows local release of therapeuticals, such as anaesthetics or antibiotics.

In this Letter we present the design and fabrication of a biodegradable polymer optical fiber that simultaneously embodies optical, microfluidic, and drug release functionalities. To the best of our knowledge, this is the first implementation of a multifunctional biodegradable fiber. The porous dual-core fiber structure presents a small inner core (which can be made hollow or filled) suspended in air by low-refractive-index water-soluble particles separating it from the larger outer core [Fig. 1(a)]. Such a geometry potentially permits many of the above-mentioned applications: the double-core structure allows efficient laser power delivery and improved collection of incoming light for passive sensing; the cladding porosity allows microfluidics, biosensing, and slow drug release by the water-soluble microstructure; a hollow core allows injection or slow release of therapeuticals. This geometry can be easily tailored to a given application by controlling the preform design and drawing processes.

The fiber preform [inset, Fig. 1(a)] was prepared by using commercially available cellulose butyrate (CB) tubes (refractive index 1.475) of two different diameters. Values for the inner/outer diameters of the smaller and larger tubes are (1/8)/(1/4) in., and (3/8)/(5/8) in., respectively. The smaller-diameter tube, which forms the inner of the two fiber cores,

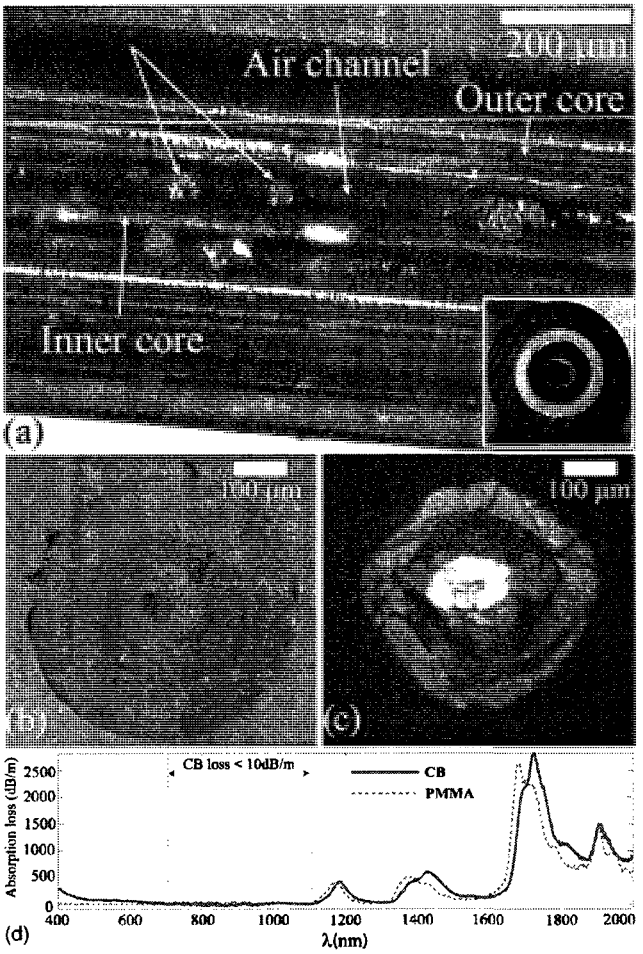

Fig. 1. (Color online) (a) Double-core biodegradable microstructured fiber. The inner core is suspended in air by the powder particles. Inset, preform cross section. (b) Fiber cross section. (c) Power distribution in the fiber cross section after 3 cm of propagation. (d) CB and PMMA material losses.

was sealed at both ends with Teflon tape and placed in the middle of the larger tube that formed the outer core. In the final fiber structure the air hole of the inner tube could be collapsed or left open, depending on the application, by controlling fiber drawing conditions. Space between the tubes was then filled with a polydisperse hydroxypropyl cellulose powder (refractive index of 1.337) to yield a lower-index inner cladding. The glass transition temperatures of CB and hydroxypropyl cellulose are 95 °C and 120 °C, respectively. As the powder has a significantly higher melting temperature than the tubes, it remained in a powder state during the drawing process. The preform was preheated at a temperature of 150 °C for one hour, and the fiber was subsequently drawn at 180 °C. Reminiscently, Kominsky *et al.*[25] used silica powder packed between two silica tubes to draw fiber featuring randomly distributed continuous holes formed by drawn gas bubbles while the powder particles were completely melted.

The biodegradable fiber was drawn down to a diameter of 450 μm [cross section shown in Fig. 1(b)], and a standard cutback measurement was performed at $\lambda = 630$ nm, resulting in a fiber transmission loss between 1 and 2 dB/cm, showing significant variation from one sample to another because of the random realization of the microstructure. A typical distribution of power in the fiber cross section after 3 cm of propagation is shown in Fig. 1(c), where the distortion in the power distribution is due mostly to the imperfect cutting of a fiber end. Powder particles remained intact during the drawing process and are clearly seen in Fig. 1(a) to be supporting the inner core and forming a very porous inner cladding with an effective refractive index close to that of air. In Fig. 1(d) ellipsometric measurements of the material losses of thick samples (~5 mm) of CB and polymethyl methacrylate (PMMA, for comparison) are presented. At $\lambda = 630$ nm, the CB material loss is 0.4 dB/cm, accounting for almost one half of the measured fiber loss. The CB transparency window (material loss <10 dB/m) is $700\ \text{nm} \lesssim \lambda \lesssim 1100$ nm, for which several medical lasers exist. In this window several meters of CB fiber can be used, long enough for many medical applications. Overall, in the near-IR the CB and PMMA material losses are similar, while in the visible the PMMA transparency window is wider, $410\ \text{nm} \lesssim \lambda \lesssim 1100$ nm.

Given the potential for *in vivo* applications that is due to the general biocompatibility of a cellulose material, it is important to understand the effects of water exposure on the fiber microstructure and fiber optical transmission. Particularly, since the powder particles in the porous cladding are made of water dissolvable hydroxypropyl cellulose, we expect dramatic changes in the fiber properties after water exposure. We used the setup illustrated in Fig. 2(a) to measure optical transmission through the fiber immersed in deionized water. The fiber passes through a capillary embedded in the window of a receptacle (recipient) such that one fiber extremity remains dry while the other extremity is immersed in water. Light from a He–Ne laser is coupled by a lens into the dry end. Two caches and an iris ensure that only light transmitted from the fiber reaches the detector. The cache within the receptacle hides only half of the output window, leaving a clear viewpoint so that a time-lapse camera can take photographs of the light side scattered by the fiber [Fig. 2(b)]. The experiment begins when the receptacle is filled with water, immersing the fiber. Figure 2(c) shows the typical variation of a transmitted power over the course of 26 h. In the first hours of an experiment, while the fiber becomes filled with water, we typically observe an increase in the fiber transmission. Transmission levels off eventually, once the fiber is filled. On removing the fiber from the receptacle, inspection under a microscope confirms the dissolution of the powder particles after 1 day of submersion. We suspect that the intake of water increases fiber transmission because water ($n = 1.33$) substitutes for air ($n = 1$) in the porous inner cladding formed by powder particles ($n = 1.337$), thus increasing the uniformity of the microstructured cladding and reducing the side scattering.

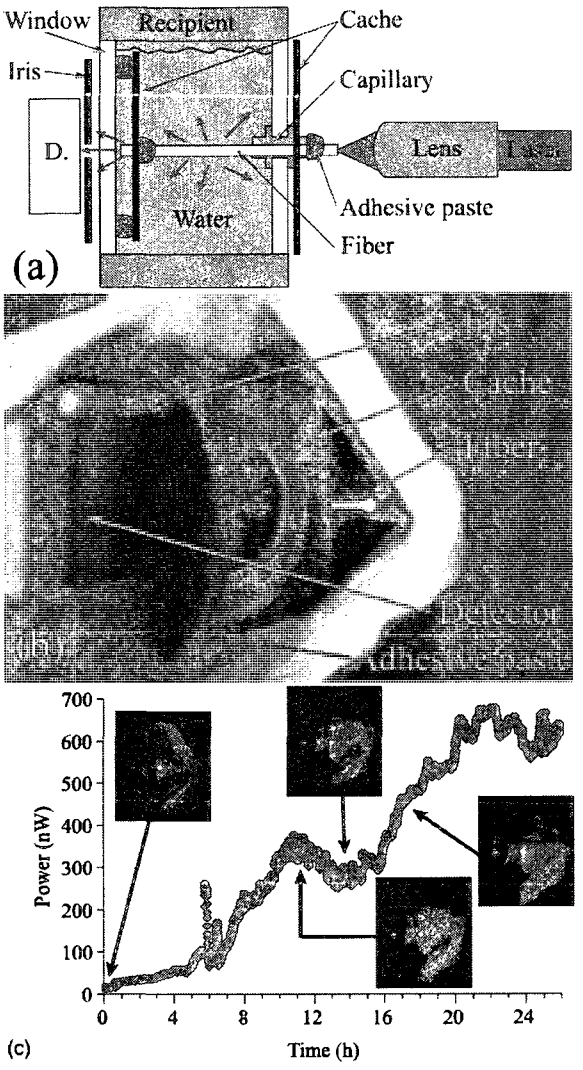

Fig. 2. (Color online) (a) Schematic of a water immersion setup. (b) Photograph of a setup. (c) Variation of transmitted power as a function of time. Insets, stills from a time-lapse camera showing the side-scattered light.

In conclusion, we have demonstrated fabrication of a novel microstructured polymer optical fiber from two types of biodegradable cellulose that have different glass transition temperatures. The resulting fiber has a porous double-cladding structure in which the inner core is suspended in the middle of an outer cladding by the intact powder particles. The inner core is a cellulose tube with a hole that can be collapsed, for laser delivery, or left open, for potential drug delivery. We have also shown that transmission through the fiber first increases when it is filled with water, leveling off when fiber is filled completely and the microstructure is dissolved. Finally, we believe that the use of monodisperse particles with a judicial choice of particle size could allow further tailoring the properties of such fibers for a variety of applications.

We thank R. Vallée and R. Maciejko for their contributions, as well as Canada Research Chairs and Canadian Institute for Photonic Innovations projects FP3 and BP5 for financial support. M. Skorobogatiy's e-mail address is maksim.skorobogatiy@polymtl.ca.

References

1. T. M. Monro, W. Belardi, K. Furusawa, J. C. Baggett, N. G. R. Broderick, and D. J. Richardson, Meas. Sci. Technol. **12**, 854 (2001).
2. J. M. Fini, Meas. Sci. Technol. **15**, 1120 (2004).
3. C. Charlton, B. Temelkuran, G. Dellemann, and B. Mizaikoff, Appl. Phys. Lett. **86**, 194102 (2005).
4. S. O. Konorov, A. M. Zheltikov, and M. Scalora, Opt. Express **13**, 3454 (2005).
5. S. P. Tai, M. C. Chan, T. H. Tsai, S. H. Guol, L. J. Chen, and C. K. Sun, Opt. Express **12**, 6122 (2004).
6. A. Argyros, I. M. Bassett, M. A. van Eijkelenborg, N. A. P. Nicorovici, R. C. McPhedran, C. M. de Sterke, M. C. J. Large, and J. Zagari, Opt. Express **9**, 813 (2001).
7. M. A. van Eijkelenborg, M. C. J. Large, A. Argyros, J. Zagari, S. Manos, N. A. Issa, I. Bassett, S. Fleming, R. C. McPhedran, C. M. de Sterke, and N. A. P. Nicorovici, Opt. Express **9**, 319 (2001).
8. A. Argyros, M. A. van Eijkelenborg, M. C. J. Large, and I. M. Bassett, Opt. Lett. **31**, 172 (2006).
9. G. Pickrell, W. Peng, and A. Wang, Opt. Lett. **29**, 1476 (2004).
10. C. Martelli, J. Canning, K. Lyytikainen, and N. Groothoff, Opt. Express **13**, 3890 (2005).
11. T. M. Monro, P. J. Bennett, N. G. R. Broderick, and D. J. Richardson, Opt. Lett. **25**, 206 (2000).
12. B. Temelkuran, S. D. Hart, G. Benoit, J. D. Joannopoulos, and Y. Fink, Nature **420**, 650 (2002).
13. G. Dellemann, T. D. Engeness, M. Skorobogatiy, and U. Kolodny, Photonics Spectra **37**, 60 (2003).
14. J. A. Harrington, Fiber Integr. Opt. **19**, 211 (2000).
15. Y. W. Shi, K. Ito, Y. Matsuura, and M. Miyagi, Opt. Lett. **30**, 2867 (2005).
16. E. Pone, C. Dubois, N. Gu, Y. Gao, A. Dupuis, F. Boismenu, S. Lacroix, and M. Skorobogatiy, Opt. Express **14**, 5838 (2006).
17. F. M. Cox, A. Argyros, and M. C. J. Large, Opt. Express **14**, 4135 (2006).
18. G. Vienne, M. Yan, Y. Luo, T. K. Liang, H. P. Ho, and C. Lin, in *Conference on Lasers and Electro-optics* (Optical Society of America, 2005), paper CLEO/PR, CWM1-1.
19. P. Mach, M. Dolinski, K. W. Baldwin, J. A. Rogers, C. Kerbage, R. S. Windeler, and B. J. Eggleton, Appl. Phys. Lett. **80**, 4294 (2002).
20. J. B. Jensen, P. E. Hoiby, G. Emiliyanov, O. Bang, L. H. Pedersen, and A. Bjarklev, Opt. Express **13**, 5883 (2005).
21. L. Rindorf, P. E. Hoiby, J. B. Jensen, L. H. Pedersen, O. Bang, and O. Geschke, Anal. Bioanal. Chem. **385**, 1370 (2006).
22. B. H. Lee, L. B. Eom, J. Kim, D. S. Moon, U. C. Paek, and G. H. Yang, Opt. Lett. **27**, 812 (2002).
23. M. T. Myaing, J. Y. Ye, T. B. Norris, T. Thomas, J. R. Baker, Jr., W. J. Wadsworth, G. Bouwmans, J. C. Knight, and P. St. J. Russell, Opt. Lett. **28**, 1224 (2003).
24. L. Fu, X. Gan, and M. Gu, Opt. Express **13**, 5528 (2004).
25. D. Kominsky, G. Pickrell, and R. Stolen, Opt. Lett. **28**, 1409 (2003).